AGU PUBLICATIONS

JGR

Journal of Geophysical Research: Oceans

RESEARCH ARTICLE

10.1002/2017JC013068

Distributions, sources, and transformations of dissolved and particulate iron on the Ross Sea continental shelf during summer

Chris M. Marsay[1,2], Pamela M. Barrett[3], Dennis J. McGillicuddy Jr.[4], and Peter N. Sedwick[1]

[1]Ocean, Earth and Atmospheric Sciences, Old Dominion University, Norfolk, Virginia, USA, [2]Now at Skidaway Institute of Oceanography, University of Georgia, Savannah, Georgia, USA, [3]School of Oceanography, University of Washington and NOAA-PMEL, Seattle, Washington, USA, [4]Woods Hole Oceanographic Institution, Woods Hole, Massachusetts, USA

Key Points:
- Summertime dissolved and particulate iron concentrations are reported for all Ross Sea water masses and off-shelf Circumpolar Deep Water
- Summertime inventories of dissolved iron and particulate trace elements are strongly influenced by high concentrations near the seafloor
- Surface water concentrations of bioavailable iron are approximately doubled if biogenic pFe is considered along with dFe concentrations

Supporting Information:
- Supporting Information S1

Correspondence to:
C. Marsay,
christopher.marsay@skio.uga.edu

Citation:
Marsay, C. M., P. M. Barrett, D. J. McGillicuddy, and P. N. Sedwick (2017), Distributions, sources, and transformations of dissolved and particulate iron on the Ross Sea continental shelf during summer, *J. Geophys. Res. Oceans*, *122*, 6371–6393, doi:10.1002/2017JC013068.

Received 5 MAY 2017
Accepted 21 JUL 2017
Accepted article online 26 JUL 2017
Published online 17 AUG 2017

Abstract We report water column dissolved iron (dFe) and particulate iron (pFe) concentrations from 50 stations sampled across the Ross Sea during austral summer (January–February) of 2012. Concentrations of dFe and pFe were measured in each of the major Ross Sea water masses, including the Ice Shelf Water and off-shelf Circumpolar Deep Water. Despite significant lateral variations in hydrography, macronutrient depletion, and primary productivity across several different regions on the continental shelf, dFe concentrations were consistently low (<0.1 nM) in surface waters, with only a handful of stations showing elevated concentrations (0.20–0.45 nM) in areas of melting sea ice and near the Franklin Island platform. Across the study region, pFe associated with suspended biogenic material approximately doubled the inventory of bioavailable iron in surface waters. Our data reveal that the majority of the summertime iron inventory in the Ross Sea resides in dense shelf waters, with highest concentrations within 50 m of the seafloor. Higher dFe concentrations near the seafloor are accompanied by an increased contribution to pFe from authigenic and/or scavenged iron. Particulate manganese is also influenced by sediment resuspension near the seafloor but, unlike pFe, is increasingly associated with authigenic material higher in the water column. Together, these results suggest that following depletion of the dFe derived from wintertime convective mixing and sea ice melt, recycling of pFe in the upper water column plays an important role in sustaining the summertime phytoplankton bloom in the Ross Sea polynya.

1. Introduction

The highest rates of primary production in the Southern Ocean are concentrated around the Antarctic continental margin, where the seasonally ice-covered waters may provide important sinks for atmospheric CO_2 during summer and fall [*Arrigo et al*., 2008a, 2008b; *Shadwick et al*., 2014; *Takahashi et al*., 2009]. In some of these areas, as over much of the Southern Ocean, surface waters remain replete with macronutrients, and phytoplankton growth during the summer months, when irradiance is sufficient to sustain productivity, is likely regulated by the supply of dissolved iron (dFe), an essential micronutrient [*Arrigo et al*., 2015; *Martin et al*., 1990; *Sedwick et al*., 2000; *Sherrell et al*., 2015; *Smith et al*., 2000]. As such, there is a need to identify the sources of dFe to surface waters over the Antarctic continental shelves in order to assess the sensitivity of the associated micronutrient supply and consequent primary production to the environmental changes that are expected to accompany a warming climate [e.g., *Smith et al*., 2012].

These dFe sources are thought to include seafloor sediments and benthic detritus [*Hatta et al*., 2013; *Marsay et al*., 2014], melting sea ice [*Lannuzel et al*., 2010; *Schallenberg et al*., 2016; *Sedwick and DiTullio*, 1997], melting glacial ice and icebergs [*Gerringa et al*., 2012; *Lin et al*., 2011; *Raiswell et al*., 2006], subglacial meltwaters [*Death et al*., 2014; *Herraiz-Borreguero et al*., 2016], upwelling Circumpolar Deep Water [*McGillicuddy et al*., 2015; *Prézelin et al*., 2000; *Sedwick et al*., 2011], and deposition of iron-bearing aerosols [*Cassar et al*., 2007; *Edwards and Sedwick*, 2001; *Winton et al*., 2014]. In addition, relatively high concentrations of particulate iron (pFe) have been measured in surface waters over the Antarctic continental shelves [*Coale et al*., 2005; *Fitzwater et al*., 2000; *Planquette et al*., 2013], although the potential availability of this iron pool to phytoplankton, either directly or via conversion to dFe, remains to be established. Evidence from other oceanic regimes suggests that labile phases of pFe can significantly add to the bioavailable iron attributed to dFe

concentrations [e.g., *Brown et al*., 2012; *Milne et al*., 2017]. The relative importance of the various dFe sources is likely to vary around the Antarctic margin due to differences in shelf topography, circulation, and glacial melt rates [*Arrigo et al*., 2015]. For example, benthic sources are thought to dominate dFe supply to surface waters of the northern Antarctic Peninsula [*Measures et al*., 2013; *Wadley et al*., 2014], melting glacial ice appears to provide a major input of dFe to Amundsen Sea surface waters [*Arrigo et al*., 2015; *Gerringa et al*., 2012], whereas both benthic sources and sea ice melt provide important dFe inputs in the Ross Sea [*Gerringa et al*., 2015; *Hatta et al*., 2017; *McGillicuddy et al*., 2015].

The Ross Sea continental shelf is among the most productive regions on the Antarctic margin. Satellite-based estimates suggest that it sustains an annual average primary production of around 20 Tg C, mostly occurring between November and February [*Arrigo et al*., 2008b; *Smith et al*., 2000, 2012]. Water column iron measurements and shipboard bioassay experiments have demonstrated that low dFe concentrations (∼0.1 nM) limit phytoplankton growth rates in the Ross Sea over these summer months [*Coale et al*., 2003; *Fitzwater et al*., 2000; *Martin et al*., 1990, 1991; *Sedwick and DiTullio*, 1997; *Sedwick et al*., 2000, 2011], which is thought to limit the magnitude of annual primary production in this region [*Arrigo et al*., 2003; *Tagliabue and Arrigo*, 2005]. As early as November, dFe supplied by winter convective mixing and sea ice melting can be drawn down to concentrations below 0.1 nM, as phytoplankton biomass accumulates in the southern Ross Sea polynya [*Coale et al*., 2005; *Sedwick et al*., 2011]. Despite this apparent early depletion of dFe, satellite data reveal that primary production continues through the mid to late summer [*Arrigo et al*., 2003], which suggests that inputs of dFe to surface waters in the polynya continue during the latter part of the growing season [*Gerringa et al*., 2015; *Kohut et al*., 2017; *Kustka et al*., 2015; *Marsay et al*., 2014; *Sedwick et al*., 2011].

In this paper, we consider data on the water column distributions of dissolved and particulate iron, based on samples collected during a shelf-wide survey of the Ross Sea in austral summer 2011–2012 as part of the project "Processes Regulating Iron Supply at the Mesoscale" (PRISM). A subset of this data has previously been presented by *Marsay et al*. [2014] to assess the benthic efflux of dFe on the Ross Sea shelf and by *McGillicuddy et al*. [2015] to estimate the seasonal supply of dFe to surface waters in this region. Here we take a broader view of the extensive dFe data set (water column samples from 50 stations), together with data for pFe, hydrography, and other field observations, in an effort to better understand the sources and transformations of iron over the Ross Sea continental shelf.

2. Methods

2.1. Sampling

All water samples and hydrographic data were collected on board the research vessel ice breaker (RVIB) *Nathaniel B. Palmer* during cruise NBP12–01, from 24 December 2011 to 8 February 2012 (Figure 1). Over 570 water column samples for trace element analysis were collected at 50 stations using Teflon-lined 5 L Niskin-X samplers (General Oceanics), custom-modified for trace metal sampling and deployed on a trace-metal clean carousel unit (SeaBird Electronics) using a Kevlar line. Subsamples for dFe analysis were processed within several hours of sample collection, using filtered N_2 gas overpressure (<10 psi) and filtering the seawater through prerinsed 0.2 μm pore AcroPak Fluorodyne II filter capsules (Pall) into acid-cleaned 125 mL low-density polyethylene bottles (Nalgene). A subset of samples ($n = 254$) were subsampled for pFe and other particulate elements by filtering 0.5–4.5 L from the Niskin bottles through paired 2 and 0.4 μm polycarbonate track-etch membranes (Nuclepore) in polypropylene holders, again using filtered-N_2 overpressure, to collect two particle size fractions. In addition, near-surface water samples (∼3 m depth) were collected while underway along four transects using a trace-metal clean towfish system, as described in *Bruland et al*. [2005]. Samples for dFe ($n = 73$) and particulate trace metals ($n = 24$) were collected directly from this underway system and filtered as above. All filtered samples for the measurement of dFe were acidified to pH 1.7 with 6 N Optima ultrapure hydrochloric acid (Fisher) while at sea. Filters of particulate material were rinsed with ∼1 μM NH_4OH solution (pH 8) under pressure to reduce sea salt interferences during analysis, with the use of a pH 8 solution designed to minimize dissolution of labile particulate elements. All shipboard sample processing was carried out in a Class-100 clean van.

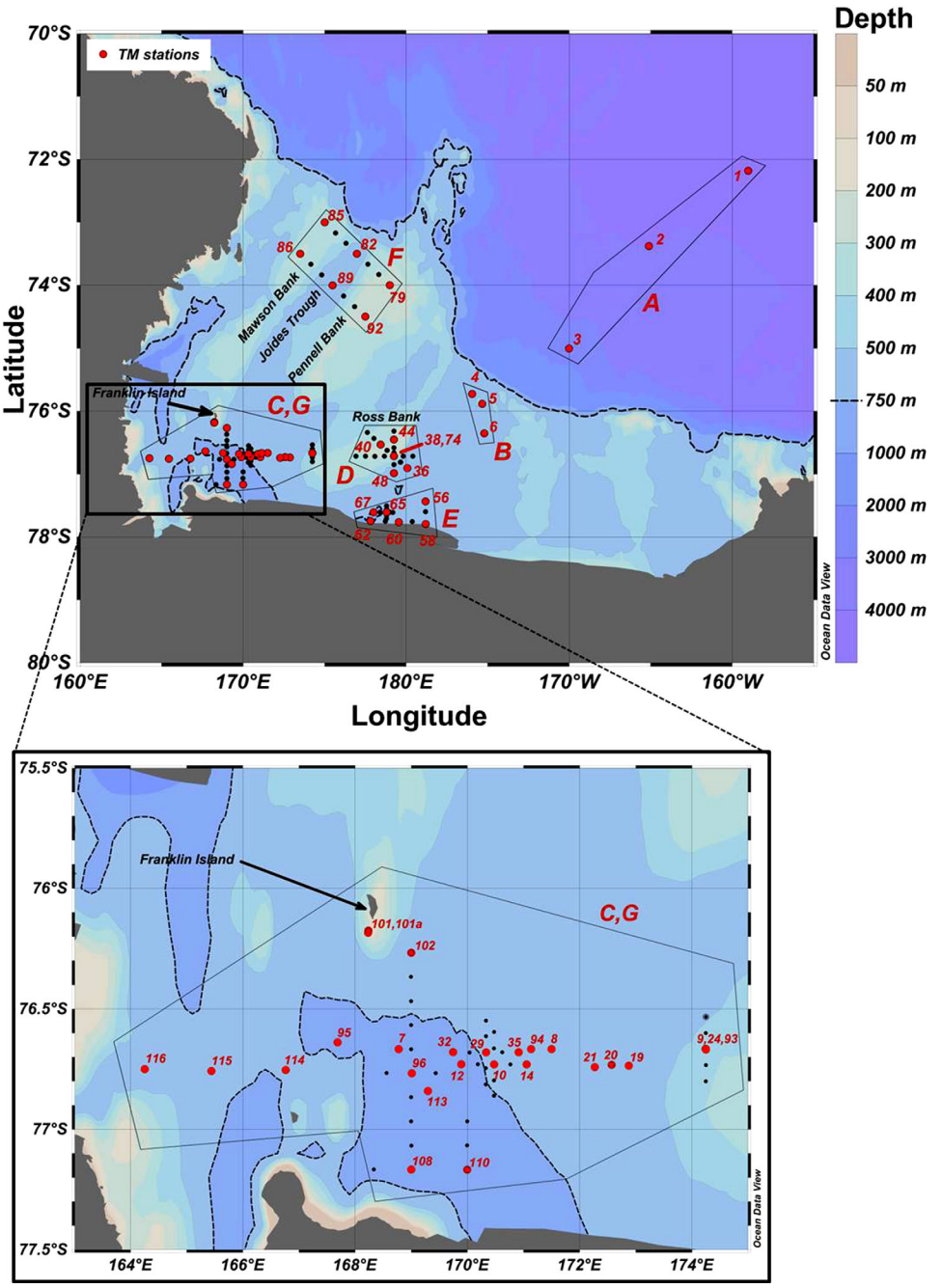

Figure 1. Bathymetric map of the Ross Sea with locations of PRISM sampling stations. Stations where dFe profiles were measured are shown in red with station numbers; stations where only hydrographic data were collected are shown in black. Black dashed line marks the 750 m depth contour. Black outlines surround stations grouped together in specific areas of interest: A, off-shelf; B, eastern Ross Sea eddies; C (and G), southwestern Ross Sea (two occupations; expanded view shown in the bottom panel); D, Ross Bank; E, Ross Ice Shelf; F, Joides Trough transects.

Hydrographic data and water samples for ancillary measurements were collected at each station using separate deployments of an SBE 911plus conductivity-temperature-depth (CTD) sensor (SeaBird Electronics) fitted on a standard rosette with twenty-four 10 L Niskin bottles.

2.2. Analysis

Shore-based dFe measurements were made following the method of *Sedwick et al*. [2005, 2011], using flow-injection analysis with inline preconcentration of dFe on resin-immobilized 8-hydoxyquinoline followed by spectrophotometric detection [*Measures et al*., 1995]. Determinations of dFe concentrations in SAFe

seawater reference materials S and D2 [*Johnson et al*., 2007] using this method were in good agreement with consensus values: analysis of SAFe S yielded a mean dFe concentration of 0.108 ± 0.008 nmol kg^{-1} ($n = 12$), while SAFe D2 gave a mean dFe concentration of 0.947 ± 0.033 nmol kg^{-1} ($n = 2$), compared to consensus values (as of May 2013) of 0.093 ± 0.008 nmol kg^{-1} and 0.933 ± 0.023 nmol kg^{-1}, respectively.

Measurements of trace metals and phosphorus in particulate material were carried out by energy-dispersive X-ray fluorescence spectroscopy following the method described by *Barrett et al*. [2012], with detection limits for pFe, pAl, pMn, and pP of 0.06, 1.27, 0.08, and 0.2 nM, respectively. Concentrations of dissolved inorganic nitrate plus nitrite (N+N), phosphate (DIP), and silicic acid (Si) were measured at sea using standard autoanalyser techniques, and chlorophyll *a* (Chl *a*) was determined using standard fluorometric methods [*Knap et al*., 1996].

3. Results

The stations occupied during the PRISM cruise are shown in Figure 1. They can be roughly grouped together based on features of interest and regions occupied, and include: three off-shelf stations (stations 1–3), two of which had current or recent sea ice coverage; three stations in and around two eddies in the eastern Ross Sea (stations 4–6); four transects across Ross Bank (stations 36–55, 72–78); several stations adjacent to the Ross Ice Shelf (stations 56–71); two transects across the Joides Trough between Pennell Bank and Mawson Bank (stations 79–92); and a number of stations in the southwestern Ross Sea occupied on 13–19 January (stations 7–35) or from 31 January to 5 February (stations 93–116). The latter stations included sites that were covered by sea ice during the initial sampling, as well as stations in close proximity to Franklin Island.

3.1. Hydrography, Chlorophyll, and Nutrients

Figure 2 displays hydrographic data (temperature, salinity, and dissolved oxygen), N+N concentrations and Chl *a* concentrations from the PRISM study as a station-based section, with stations grouped together in the regions described above, and station number in each region increasing from left to right.

Off-shelf stations 1–3 provided an opportunity to sample the relatively warm, saline Circumpolar Deep Water (CDW) at depths of >300 m, which was also clearly defined by low dissolved oxygen concentrations (Figure 2). In addition, these stations were situated offshore (station 1), within (station 2) and inshore (station 3) of a band of sea ice that spanned the northeastern perimeter of the Ross Sea Polynya at the time of our approach in early January. All three off-shelf stations were characterized by relatively low Chl *a* concentrations (0.33–1.16 μg L^{-1}) and high macronutrient concentrations (26.1–29.3 μM N+N) in the surface mixed layer (Table 1).

Over the continental shelf, the polynya was already extensive when our first stations were occupied, as is typical of the Ross Sea in January [*Smith et al*., 2012]. Most stations had experienced <10% sea ice coverage for several days prior to occupation, with notable exceptions being several stations near the Ross Ice Shelf and in the southwestern Ross Sea (supporting information Figure S1). Water temperatures on the shelf ranged from −2.1 to +2.5°C, and salinity ranged from 32.8 to 34.8 (Figure 3), which are typical of the Ross Sea climatology [see *Orsi and Wiederwohl*, 2009, Figure 2], and all six of the major Ross Sea water masses described by *Orsi and Wiederwohl* [2009] were sampled during this study (Figure 3 and Table 2). Mixed layer depths, calculated by an increase in sigma-theta of 0.02 kg m^{-3} from surface values, ranged from 4 to 114 m, with a median depth of 22 m (Table 1).

Compared to the off-shelf stations, stations 4–6 in the eastern Ross Sea were characterized by a warmer, more saline mixed layer, with lower macronutrient concentrations and higher Chl *a* concentrations (Table 1 and Figure 2). Surface waters at stations 4 and 6, both near the center of cyclonic eddies, were warmer (–0.2 to +0.2°C), had elevated Chl *a* (6.2–13.5 μg L^{-1}) and were depleted in macronutrients (18–23 μM N+N), relative to station 5, which was located outside of the eddies (–0.5°C, 4.0 μg L^{-1} Chl *a* and 26 μM N+N).

During our initial sampling of stations in the southwestern Ross Sea (stations 7–35), a series of transects were performed. These included an eastward transect from the ice edge in the west (station 7 at 168.8°E; mixed layer temperature −0.5°C and salinity 33.1) into warmer (+0.7 to +2.4°C), more saline waters

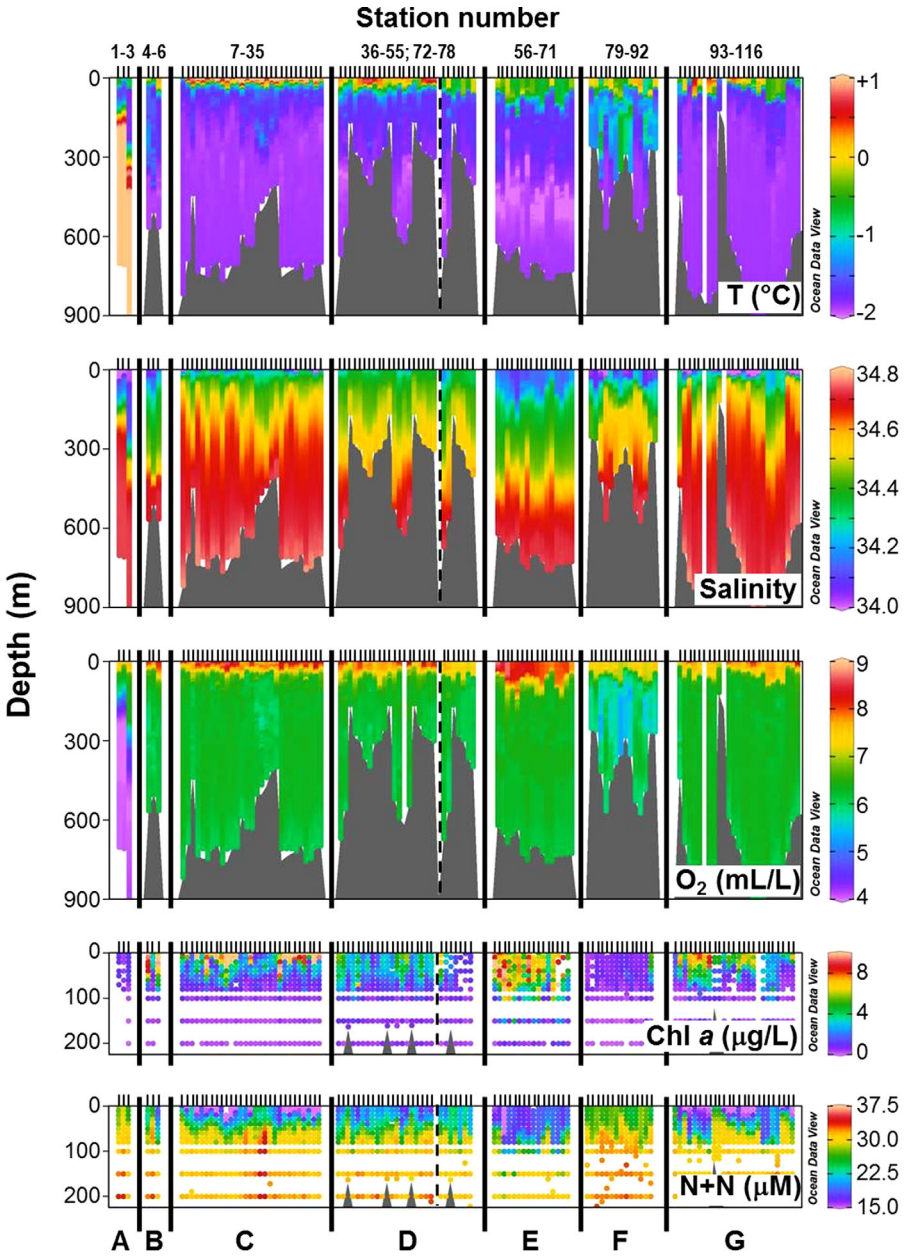

Figure 2. Sections showing depth profiles of temperature, salinity, dissolved O_2, chlorophyll *a*, and nitrate + nitrite (N+N) for study areas A–G, separated by solid black lines. Station number increases from left to right in each study area, with individual stations shown by tick marks at regular spacing. Areas A–G, defined in Figure 1, are A, off-shelf stations (stations 1–3); B, eastern eddy stations (stations 4–6); C, southwestern Ross Sea (stations 7–35); D, Ross Bank (stations 36–55 and 72–78, separated by black dashed line); E, Ross Ice Shelf (stations 56–71); F, Joides Trough transects (stations 79–92); G, second visit to southwestern Ross Sea (stations 93–116).

(stations 8 and 9), and a short east-to-west transect across a frontal region (stations 19–21), both of which revealed pronounced zonal gradients in surface macronutrient and chlorophyll concentrations, with higher biomass in the west. Two surveys (stations 10–14 and 29–35) of a cyclonic eddy within the high biomass region showed upward doming of the pycnocline at depth at the eddy center (supporting information Figure S2). During our second visit to this area (stations 93–116), which included stations as far east as the initial occupation, and additional stations as far west as 164.3°E, the surface mixed layer was generally cooler and fresher (Table 1). Surface temperatures ranged from −0.68 to +0.63°C for most stations, but were colder (–1.89 to −0.48°C) and also fresher at the four westernmost stations (stations 95 and 114–116), which had been covered to varying extents by sea ice during the earlier visit, and at the Franklin Island stations

Table 1. Regional Ranges in Mixed Layer (ML) Depth and Station ML-Averaged Values of Potential Temperature, Salinity, Chlorophyll (Chl *a*), Dissolved Inorganic Nitrogen (N+N), dFe and pFe Concentrations

Study Area[a]	ML Depth (m)	Pot. Temp (°C)	Salinity	Chl *a* (μg L^{-1})	N+N (μM)	dFe (nM)	pFe (nM)
Off-shelf	16–48	−1.1 to −0.5	33.67–34.01	0.3–1.0	26.7–29.3	0.05–0.44	1.1–2.5
Eastern Ross Sea	17–26	−0.6 to +0.2	34.03–34.19	3.4–9.9	18.7–26.5	0.28–0.35	1.8–3.4
SW Ross Sea 1	5–32	−0.5 to +2.5	33.14–34.33	0.9–20.8	7.1–24.5	0.04–0.11	1.2–5.7
Ross Bank	7–74	−0.7 to +0.7	34.19–34.39	0.8–6.4	17.1–24.4	0.04–0.08	1.3–3.4
Ice Shelf	22–114	−0.7 to +0.0	34.09–34.21	3.5–10.8	14.4–19.9	0.06–0.08	2.0–4.8
Joides Trough	14–68	−1.3 to +0.2	33.87–34.27	0.3–4.9	24.9–28.0	0.04–0.07	1.2–1.6
SW Ross Sea 2	4–97	−1.2 to +0.6	32.82–34.30	1.5–9.0	11.3–25.7	0.04–0.06	1.4–3.8

[a]As defined in Figure 1. SW Ross Sea 1 and 2 consist of stations 7–35 and 93–116, respectively.

(stations 101 and 101a), which still had partial ice cover when occupied (supporting information Figure S1). Mixed layer Chl *a* concentrations were again variable in the region, but typically lower than during the first visit (Figure 2).

Stations sampled during transects across Ross Bank (stations 36–55) revealed some of the saltiest surface mixed layer waters encountered during the cruise, which cooled and freshened as the mixed layer deepened over a period of 6 days before being reoccupied (stations 72–78; Figure 2). Mixed layer N+N concentrations ranged from 17–24 μM and Chl *a* concentrations spanned 0.8–6.4 μg L^{-1}. In contrast, stations near the Ross Ice Shelf (stations 56–71) typically had deeper, fresher, and colder surface mixed layers, which were more depleted in macronutrient concentrations and exhibited some of the highest Chl *a* concentrations measured during our study [*Li et al.*, 2017; *Smith et al.*, 2017]. The two transects across the Joides Trough (stations 79–92) revealed surface waters distinguished by generally high macronutrient concentrations (25–28 μM N+N) and by low Chl *a* (0.3–0.9 μg L^{-1}), with the exception of station 92 over the southwestern part of Pennell Bank (4.9 μg L^{-1} Chl *a*).

3.2. Dissolved Iron

Concentrations of dFe in water column samples ranged from 0.03 to 2.19 nM (Figures 3 and 4), with the majority of stations showing very low (<0.1 nM) concentrations in surface waters and an increase in

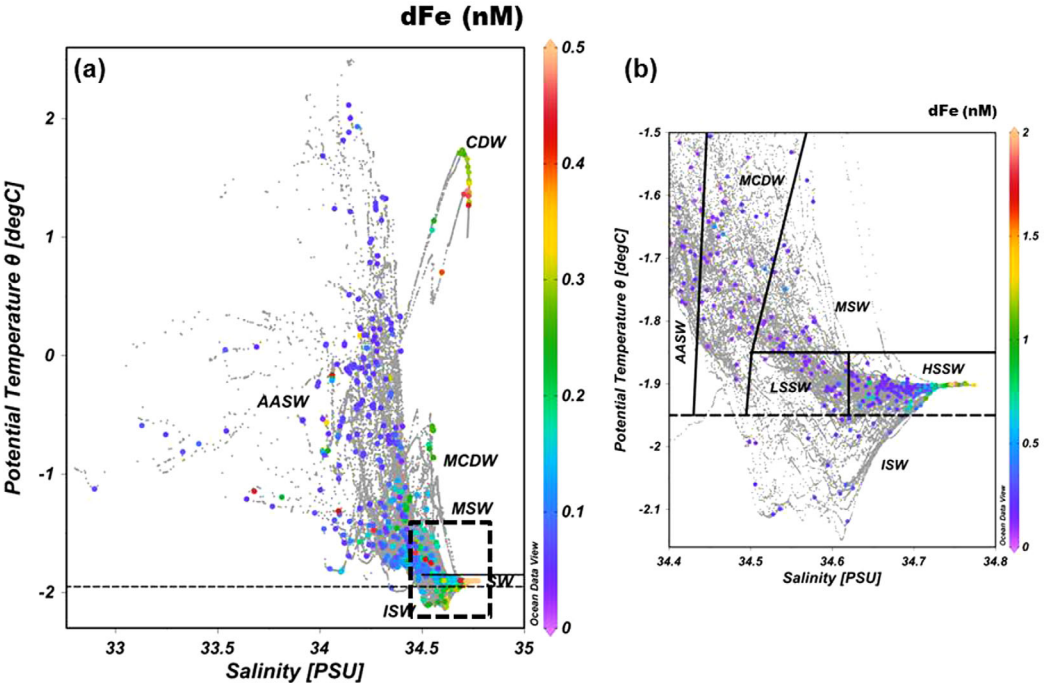

Figure 3. Dissolved iron (dFe) concentrations measured during PRISM (colored dots) as a function of salinity and potential temperature (θ), overlain upon all temperature and salinity data generated during PRISM (gray dots). (a) Full range of salinity and θ, with horizontal lines marking the upper θ limits of ISW (–1.95°C) and of SW (–1.85°C). (b) Expanded view of cold, dense waters, with lines included to define the different water masses (defined in text). Note the different dFe scale in Figure 3b.

Table 2. Dissolved and Particulate Iron Concentrations of Different Ross Sea Water Masses

Water Mass	dFe Range (nM)	dFe Mean ± SD (nM)	*n*	pFe Range (nM)	pFe Mean ± SD (nM)	*n*
Surface ML	0.03–0.44	0.08 ± 0.08	91	0.63–6.2	2.6 ± 1.3	41
AASW	0.03–0.45	0.10 ± 0.07	249	0.68–18.7	3.0 ± 2.7	108
SW/MSW	0.06–2.19	0.35 ± 0.34	237	0.93–57.3	8.7 ± 12.3	91
MSW	0.06–0.50	0.16 ± 0.11	35	0.93–6.3	2.8 ± 1.6	15
LSSW	0.07–0.56	0.17 ± 0.10	29	1.2–9.8	3.9 ± 3.1	10
HSSW	0.10–2.19	0.45 ± 0.39	153	1.4–57.3	12.0 ± 14.5	57
ISW	0.13–0.36	0.24 ± 0.07	20	1.2–5.3	2.7 ± 1.5	9
CDW/MCDW	0.05–0.48	0.20 ± 0.11	84	0.83–10.7	2.8 ± 2.0	48
CDW	0.26–0.47	0.34 ± 0.08	16	0.83–2.7	1.53 ± 0.52	15
MCDW[a]	0.05–0.48	0.16 ± 0.09	68	1.1–10.7	3.8 ± 2.1	33

[a]Excluding two stations near Franklin Island.

concentration with depth. The pervasive low dFe concentrations in the upper 50 m at the on-shelf stations (mean = 0.08 ± 0.07 nM; $n = 170$) were consistent with near-surface dFe concentrations of towfish samples (0.05–0.19 nM, mean = 0.08 ± 0.02 nM; supporting information Figure S3). These data agree with previous studies, in which dFe concentrations of <0.2 nM have been measured in Ross Sea surface waters [*Coale et al*., 2005; *Fitzwater et al*., 2000; *Gerringa et al*., 2015; *Sedwick et al*., 2000, 2011], and are not surprising given the mid to late summer timing of our cruise, by which time satellite-derived chlorophyll climatology shows that 2 months of intense primary production have typically occurred [*Smith et al*., 2012]. Such low dFe concentrations are generally considered to limit phytoplankton growth, and incubation experiments conducted during the PRISM cruise confirmed widespread iron-limited conditions [*Ryan-Keogh et al*., 2017].

The generally uniform dFe distribution contrasts with macronutrient concentrations in AASW, which were much more variable in the upper 50 m (e.g., N+N panel in Figure 2), and measured dFe showed no strong relationships with macronutrient or chlorophyll *a* concentrations in surface waters (supporting information Figure S4), or with photosynthetic efficiency [*Ryan-Keogh et al*., 2017]. We ascribe this to spatial and temporal variations in the supply and removal of dFe and macronutrients, which are not necessarily coupled [*McGillicuddy et al*., 2015].

For stations of at least 400 m depth, low dFe concentrations often persisted throughout the upper 100 m, before increasing deeper in the water column. However, at some stations, notably those near the Ross Ice Shelf and at some locations in the southwestern polynya, concentrations of ~0.1 nM extended as deep as 200 m, likely as a result of the deeper mixed layers in those areas. In contrast, midwater dFe concentrations (100–300 m depth) were often higher at stations with seafloor depths less than 400 m, relative to stations in deeper water, although the elevated concentrations did not extend into the surface mixed layer (Figure 4). The same was true for stations 102 and 116, despite being in relatively deep water, likely due to their relative proximity to shallow coastal waters. Station 10, in the center of a cyclonic eddy, also had slightly elevated dFe in the 200–600 m depth range compared to nearby stations (supporting information Figure S2; see section 4.1.3). The feature was less clear during a second survey of the eddy (station 29 versus stations 32 and 35).

A feature common to many of the dFe profiles is a large increase in concentrations near the seafloor, often resulting in pronounced vertical concentration gradients (Figure 4). This has been occasionally observed in several previous studies of dFe in the Ross Sea, and attributed to the release of dissolved iron from sediment pore waters and/or resuspended benthic material [e.g., *Gerringa et al*., 2015; *Hatta et al*., 2017; *Sedwick et al*., 2011]. The near-seafloor dFe gradients observed during the PRISM cruise are discussed in detail by *Marsay et al*. [2014].

3.3. Particulate Iron, Aluminum, Manganese, and Phosphorus

Total pFe concentrations in the water column were always higher than dFe, ranging from 0.68 to 57.3 nM, with most samples in the 1–5 nM range (Figure 5), and the pFe:dFe concentration ratio of water column samples averaged 28:1 (range 2.5:1–214:1, $n = 250$). Particulate iron was typically dominated by the >2 μm (hereafter "large") size fraction (68% of total pFe on average), with concentrations of 0.37–47.0 nM, while

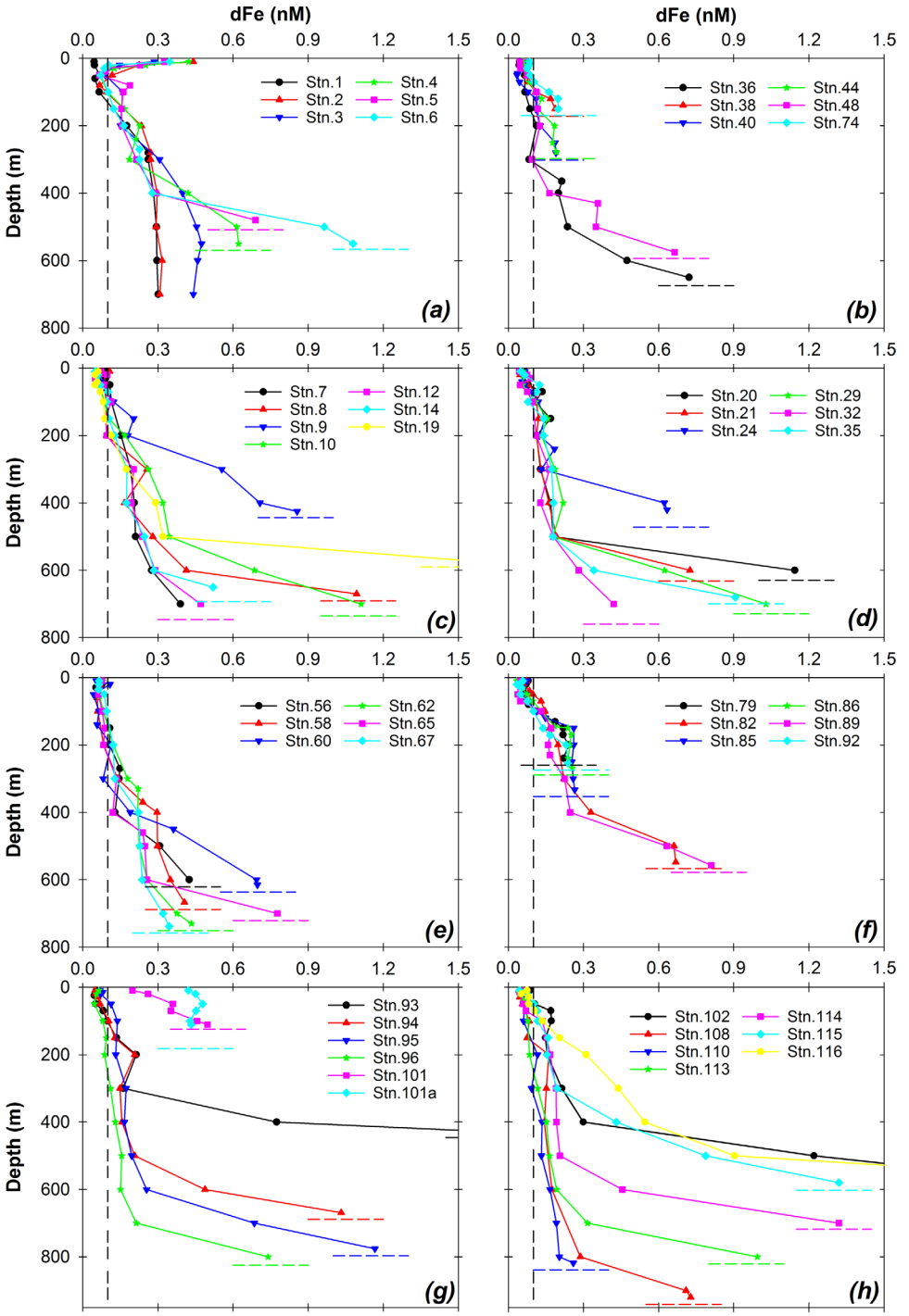

Figure 4. Depth profiles of dFe for all stations, grouped by region: (a) off-shelf and eastern Ross Sea eddy stations, (b) Ross Bank, (c, d) first visit to southwestern Ross Sea, (e) Ross Ice Shelf, (f) Joides Trough transects, (g, h) second visit to southwestern Ross Sea. Vertical dashed line marks a concentration of 0.1 nM dFe. Horizontal dashed lines represent seafloor depth at each station. Values that exceed the concentration scale are station 19, 570 m (1.51 nM); station 93, 427 m (1.57 nM); station 102, 550 m (1.84 nM) and 575 m (1.90 nM); and station 116, 560 m (2.19 nM).

material in the 0.4–2.0 μm (hereafter "small") size fraction had pFe concentrations of 0.29–35.6 nM. Analysis of particulate material collected using the towfish showed near-surface pFe concentrations of 1.3–6.1 nM (mean 2.4 ± 1.1 nM; supporting information Figure S3), and the same predominance of pFe in the large size class (72% of total pFe on average).

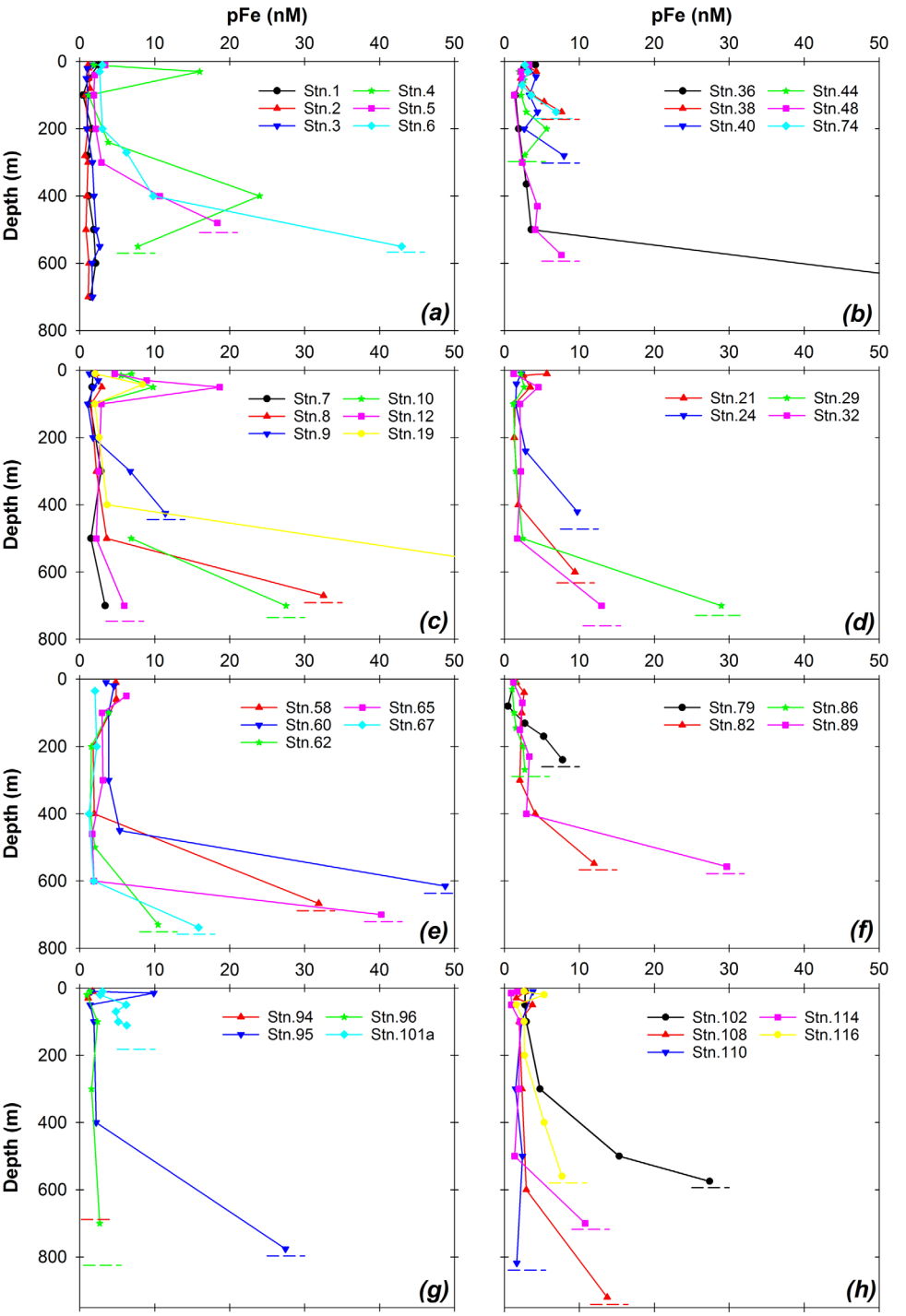

Figure 5. Depth profiles of total pFe (small and large size fractions combined) for all stations, grouped by region: (a) off-shelf and eastern Ross Sea eddy stations, (b) Ross Bank, (c, d) first visit to southwestern Ross Sea, (e) Ross Ice Shelf, (f) Joides Trough transects, (g, h) second visit to southwestern Ross Sea. Horizontal dashed lines represent seafloor depth at each station. Values that exceed the concentration scale are station 19, 570 m (55.1 nM); and station 36, 650 m (57.3 nM).

There have been fewer reported measurements of pFe in the Ross Sea than for dFe, although the pFe concentrations measured during the PRISM cruise fall within the wide range of previous measurements. *Fitzwater et al.* [2000] and *Coale et al.* [2005] reported total pFe concentrations of 0.12–6.5 and 0.13–97 nmol kg^{-1}, respectively, and *Hatta et al.* [2017] measured pFe concentrations of 0.05–8.8 nM in 0.8–51 μm sized material. *Sedwick et al.* [2011] calculated acid-labile particulate iron concentrations of 0.02–68 nM by the

difference from iron measured in acidified filtered and unfiltered samples, with the latter assumed to include all pFe except that contained in refractory aluminosilicate particles.

The vertical distributions of total pFe were largely similar to dFe, with low concentrations (3.1 ± 2.7 nM; $n = 103$, including towfish samples) in the upper 50 m, and higher concentrations near the seafloor (Figure 5), with this trend followed for both particulate size fractions (see supporting information Table S1). These distributions are consistent with previous data from the Ross Sea, for the small number of stations that have been sampled close to the seafloor [*Coale et al*., 2005; *Fitzwater et al*., 2000; *Sedwick et al*., 2011]. Vertical profiles often showed little variation in pFe over the middle water column, particularly for the small size fraction. However, some stations displayed subsurface pFe maxima in the upper 100 m, which were not seen in dFe profiles. These were particularly noticeable for stations 12 (18.7 nM pFe at 50 m depth) and 4 (16.0 nM at 30 m depth), although smaller maxima were present at stations 10, 19, and 95, among others (Figure 5). In each case, the subsurface pFe maximum was located slightly below the chlorophyll fluorescence maximum, suggesting that the elevated pFe was associated with sinking phytoplankton biomass or organic detritus. However, this pFe maximum was not observed at all stations with high subsurface fluorescence; for example, stations 4 and 6 had similar subsurface fluorescence maxima, with only station 4 showing a corresponding maximum in pFe. This may simply reflect the limited resolution of the pFe measurements, both in terms of the number of stations sampled and the depths that were sampled at each station, or it may indicate that the pFe maxima are transient features modulated by episodic vertical export of particles.

The vertical distribution of particulate aluminum (pAl) tended to mirror pFe, with generally low surface concentrations (median 20.1 nM in the upper 50 m, $n = 103$) and higher concentrations (up to 185 nM) near the seafloor (see supporting information Table S1), with occasional subsurface maxima observed (data not shown). Similarly, particulate manganese (pMn) concentrations varied from below detection limit (particularly in the small size fraction) in the upper water column to values near the seafloor averaging 0.63 ± 0.37 nM ($n = 22$), and as high as 1.4 nM (supporting information Table S1). Due to their similar distributions, there was a strong correlation between total pFe and total pAl (Spearman rank order correlation, $r_s = 0.78$, $p < 0.001$, $n = 242$), and, despite many pMn concentrations in the small size class being below our limit of detection, the smaller data set of total pMn concentrations also showed strong correlations with both pFe ($r_s = 0.67$, $p < 0.001$, $n = 63$) and pAl ($r_s = 0.71$, $p < 0.001$, $n = 63$).

In contrast, particulate phosphorus (pP) typically showed a significant decrease with depth, from maximum concentrations of 10.8–404 nM (median 50.6 nM, $n = 101$) in the upper 50 m, to lower and less variable concentrations of 5.4–42.0 nM (median 8.8 nM, $n = 58$) below 200 m depth (supporting information Table S1), as expected for an essential nutrient element. Total pP showed a strong correlation with Chl *a* over the upper 200 m ($r_s = 0.763$, $p < 0.001$, $n = 120$), driven by both parameters displaying variable concentrations in the upper 50 m, a decrease with depth and much less variability by 200 m.

3.4. Particulate Element Ratios

Elemental ratios of particulate material can be useful in determining composition of particles, in terms of lithogenic, biogenic and authigenic material. In this study, measured ratios of pP/pAl throughout the water column averaged 3.7 ± 2.5 mol mol^{-1} and 1.4 ± 1.8 mol mol^{-1} in the small and large fractions, respectively. These values are substantially greater than the average ratio found in upper continental crust (UCC; 0.0075 mol mol^{-1} [*Wedepohl*, 1995]), confirming the biogenic nature of most pP. The contrasting distributions in pP and pFe are evident from pFe/pP ratios, which increased with depth (Figures 6a and 6b and supporting information Table S1) from upper 50 m median values of 0.034 and 0.066 mol mol^{-1} in the small and large size fractions to median values of 0.52 and 10.3 mol mol^{-1} within 50 m of the seafloor. In general, the pFe/pP ratio of the large size fraction was greater than that of the small size fraction, and had the most dramatic increase toward the seafloor.

The ratio of pFe/pAl ranged from 0.07 to 0.65 mol mol^{-1} in the small size class, with a median of 0.23 mol mol^{-1} ($n = 266$; Figure 6c), and from 0.01 to 0.63 mol mol^{-1} in the large size class, with a median of 0.26 mol mol^{-1} ($n = 265$; Figure 6d). Both median values are close to the average UCC Fe/Al ratio of 0.19 mol mol^{-1} [*Wedepohl*, 1995] and the Fe/Al ratio of Ross Sea surface sediments (0.24 mol mol^{-1} [*Angino*, 1966]), In both size classes, pFe/pAl showed an increasing trend toward the seafloor (Figures 6c and 6d and supporting information Table S1).

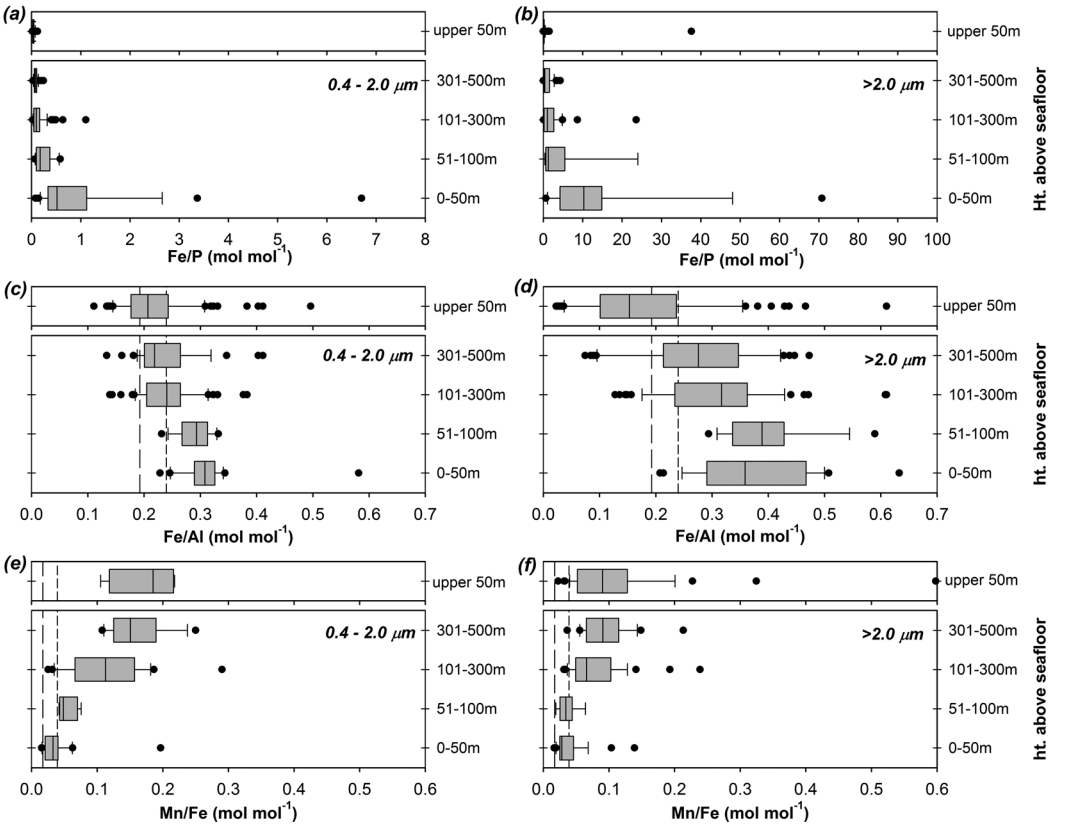

Figure 6. Box and whisker plots for elemental molar ratios in particulate material from surface waters (upper 50 m) and within height intervals above the seafloor for all on-shelf stations: (a, b) pFe/pP in small and large size fractions, (c, d) pFe/pAl in small and large size fractions, and (e, f) pMn/pFe in small and large size fractions. Each box spans the 25th to 75th percentiles and is bisected by the median; "whiskers" cover the 10th to 90th percentiles; black dots represent the remaining data points. Long dash and short dash vertical lines in *c–f* represent corresponding global crustal average [*Wedepohl*, 1995] and Ross Sea surface sediment [*Angino*, 1966] molar ratios, respectively.

Due to the large number of upper ocean pMn values below the detection limit in the upper ocean, the distributions of pMn/pAl and pMn/pFe are biased toward deeper measurements, particularly for the smaller size fraction. With this caveat in mind, the pMn/pAl ratios in the small and large size fractions ranged from 0.005 to 0.068 mol mol^{-1} and 0.003 to 0.065 mol mol^{-1}, respectively, with median values of 0.027 mol mol^{-1} ($n = 74$) and 0.018 mol mol^{-1} ($n = 163$). These compare to an UCC value of 0.003 mol mol^{-1} [*Wedepohl*, 1995] and an average value of 0.009 mol mol^{-1} for Ross Sea surface sediments [*Angino*, 1966]. For both size fractions, values were close to surface sediment values near the seafloor. The small size fraction pMn/pAl displayed a clear increase with height above the bottom, though the trend was less clear for the large size fraction (supporting information Table S1).

The pMn/pFe ratio was also generally enriched relative to both the UCC ratio of 0.017 mol mol^{-1} [*Wedepohl*, 1995] and the local surface sediment ratio of 0.039 mol mol^{-1} [*Angino*, 1966] (Figures 6e and 6f). Our pMn/pFe ratios ranged from 0.015 to 0.290 mol mol^{-1} (median 0.110 mol mol^{-1}) in the small size fraction, and from 0.016 to 0.665 mol mol^{-1} (median 0.082 mol mol^{-1}) in the large size fraction (supporting information Table S1). As for pMn/pAl, the values of pMn/pFe were typically closest to crustal and sediment ratios within 50 m of the seafloor and tended to increase higher in the water column.

4. Discussion

4.1. Iron Concentrations of the Major Ross Sea Water Masses

The Ross Sea is characterized by a surface inflow of cold, fresh Antarctic Surface Water (AASW) from the east, which forms dense, saline Shelf Water on the continental shelf with winter cooling and sea ice formation [*Orsi and Wiederwohl*, 2009]. Shelf Water (SW) is further classified by salinity as Low Salinity Shelf Water

(LSSW), which forms mainly in the eastern Ross Sea, and High Salinity Shelf Water (HSSW), which is formed mostly in the western Ross Sea. Ice Shelf Water (ISW) is formed when water in contact with the underside of the Ross Ice Shelf is supercooled below the surface freezing temperature [*Smethie and Jacobs*, 2005]. Relatively warm, salty, and oxygen-poor CDW, which circulates round the Antarctic continental slope, mixes with AASW near the shelf break and intrudes on to the Ross Sea continental shelf at depth as Modified Circumpolar Deep Water (MCDW) [*Orsi and Wiederwohl*, 2009]. The poleward flow of MCDW follows local bathymetric features, notably the north-south trending troughs [*Dinniman et al*., 2011; *Kohut et al*., 2013], and undergoes further mixing with AASW. On-shelf mixing of MCDW and SW produces Modified Shelf Water (MSW), a dense, transitional water mass that is warmer than SW.

In the following sections, we consider the water column distributions of dFe and pFe during the PRISM cruise in relation to the different water masses present. In doing so, we identify water masses following *Orsi and Wiederwohl* [2009], by using neutral density (γ^n) to distinguish CDW/MCDW from the upper layer AASW and from the lower layer SW/MSW. Further water mass definitions are described below. Our analysis indicates that much of the water column inventories of dFe and pFe reside within the dense shelf waters, with lowest dFe concentrations in AASW, despite some localized high concentrations. The ISW and CDW are both shown to be enriched in dFe but not pFe, relative to surface waters, while the MCDW has higher pFe but lower dFe than CDW.

4.1.1. Iron in Antarctic Surface Water

Nearly half of the samples collected for dFe measurements during PRISM were from AASW, defined as having $\gamma^n < 28.0$ kg m^{-3} [*Orsi and Wiederwohl*, 2009]. This water mass accounted for the upper 100 m of the water column at the majority of stations (except at several in the southwestern Ross Sea), and sometimes extended as deep as 200–300 m (Figure 7a). Unsurprisingly for waters that comprise the surface mixed

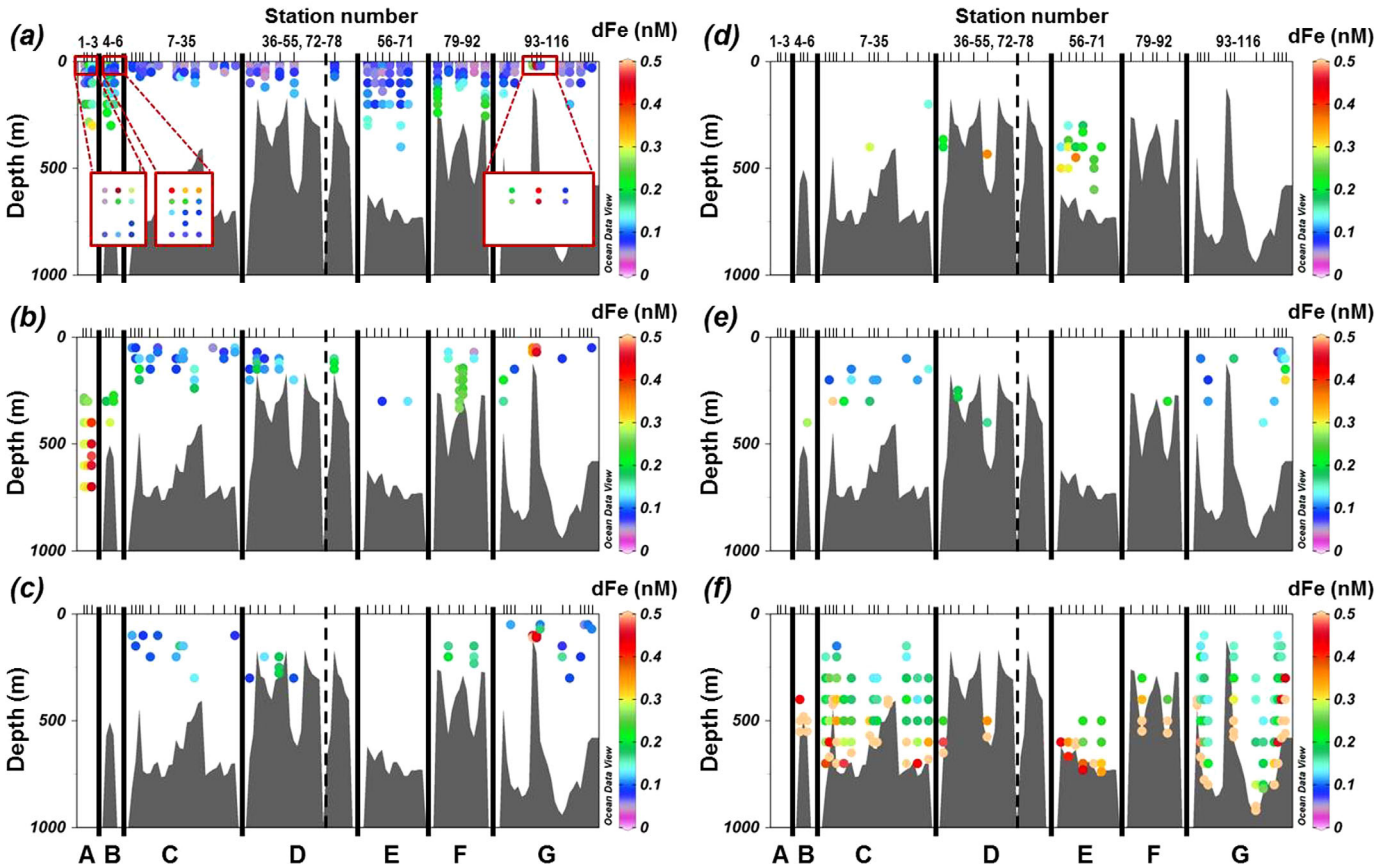

Figure 7. Dissolved iron measurements in different Ross Sea water masses, sampled in the geographical areas A–G (see Figure 1) and displayed in sections corresponding to Figure 2. Water masses are (a) AASW, (b) CDW (region A only) and MCDW, (c) MSW, (d) ISW, (e) LSSW, (f) HSSW. Pink dots in Figure 7f denote dFe concentrations of >0.5 nM (as high as 2.2 nM). Enlarged boxes in Figure 7a show upper 50 m concentrations for (left to right) stations 1–3, stations 4–6, and stations 101, 101a, and 102. An expanded version of Figure 7a is shown in supporting information Figure S5.

layer, where biological uptake draws dFe down to subnanomolar concentrations, AASW had the lowest average dFe concentrations of the water masses sampled (0.10 ± 0.07 nM, $n = 249$; Table 2). Exceptions to this included waters above Pennell Bank, where AASW extended to the seafloor (0.2–0.25 nM at depths of ~150–250 m), and surface waters at offshore stations 2 and 3, and stations 4–6 on the outer shelf (see below). The highest AASW dFe concentrations were measured at station 101 near Franklin Island (0.45 nM at 20 m depth; Figures 4 and 7a), which is discussed in more detail in section 4.2.

The elevated near-surface dFe concentrations at stations 2 and 3 (0.3–0.4 nM at 10 m depth and ~0.2 nM at 20 m depth; Figures 4 and 6a) are most likely due to melting sea ice, which typically has dFe and pFe concentrations that are significantly higher than surface seawater [*Lannuzel et al*., 2007]. Station 2, occupied as we entered the Ross Sea, was located within a band of melting sea ice, and satellite imagery shows that station 3 had ice coverage in the days immediately prior to our occupation (supporting information Figure S1). At station 2, the surface dFe maximum was accompanied by a surface minimum in salinity. Macronutrient drawdown at both stations was small relative to other stations in the polynya, suggesting that the seasonal phytoplankton bloom had not yet developed. Therefore, as observed previously in the Ross Sea [*Fitzwater et al*., 2000; *Sedwick and DiTullio*, 1997; *Sedwick et al*., 2011], this band of melting sea ice on the northern edge of the polynya appears to have provided a localized source of dFe, but not pFe (surface concentrations of pFe at stations 2 and 3 were no higher than at station 1; Figure 5).

Stations 4–6 also had elevated surface dFe concentrations (0.1–0.4 nM in the upper 20 m; Figures 4 and 7a), and station 4 showed a large maximum in >2 μm pFe concentration just below the mixed layer (15.4 nM; Figure 5). These stations were located in two eddies that were propagating to the northeast, as indicated by underway XBT and ADCP surveys. Near the center of each eddy (stations 4 and 6), Chl *a* was elevated and mixed layer macronutrient concentrations were depleted, relative to off-shelf stations, yet dFe remained relatively high. In contrast to the vertical profile samples, dFe concentrations of near-surface underway samples collected near stations 4–6 were low (<0.1 nM; supporting information Figure S3), and similar to surface water dFe concentrations measured elsewhere during the study. This mismatch between towfish dFe and the unexpectedly high 10–30 m vertical profile dFe data remains an unexplained feature in our dataset, although the fact that elevated dFe is restricted to near-surface waters, similar to stations 2 and 3, suggests a sea ice source is most likely.

In the southwestern Ross Sea, stations 7, 10, 12, 29, and 32 also had partial or recent ice cover when they were sampled, although only station 7, close to the pack ice edge, showed an obvious surface salinity minimum (33.1–33.3 in the upper 10 m). None of these stations had dFe concentrations above 0.09 nM, although stations 10 and 12 both displayed high pFe concentrations in association with high Chl *a*. During our second visit to this area, stations 95 and 114–116, which were ice-covered during the first visit, each showed a salinity minimum (32.8–33.8) in the upper 20 m, consistent with recent melting of sea ice, but again, none of these stations had dFe concentrations above 0.08 nM in the upper 30 m. Thus, for all of the stations sampled in the southwestern Ross Sea, the proximity of melting sea ice was not associated with elevated dFe concentrations. However, high chlorophyll concentrations in this region, along with relatively low macronutrient concentrations (minimum N+N ranged from 6.8 to 17.3 μM) suggest that significant primary production had occurred prior to sampling, despite the recent sea ice cover, and this production may have already assimilated much of the dFe released from the melting sea ice. Another possible scenario, as discussed by *Lannuzel et al*. [2008], is that the sea ice in the southwestern Ross Sea had previously warmed sufficiently to allow melting and brine drainage from its upper layers, thereby releasing much of the ice-associated dFe whilst ice cover remained.

Thus, although tracer modelling simulations suggest that dFe released from melting sea ice may satisfy as much as 35% of the annual biological iron demand in the Ross Sea [*McGillicuddy et al*., 2015], we found only localized evidence of this Fe source to surface waters during our mid-summer study, consistent with most stations having been ice free for some time before sampling, and the rapid biological removal of sea ice derived iron as the polynya opens in the springtime [*Sedwick et al*., 2011].

The AASW showed no significant enrichments in surface dFe concentrations at stations close to the Ross Ice Shelf, relative to those in the central polynya, despite reports of elevated dFe in waters adjacent to other Antarctic ice shelves [*Gerringa et al*., 2012; *Sherrell et al*., 2015]. Concentrations at stations 56–67 averaged 0.07 ± 0.01 nM dFe in the upper 100 m, with a maximum of 0.11 nM (Figures 4 and 7a). The surface mixed

layer near the ice shelf was relatively cold and deep, with high Chl *a* concentrations and substantial macronutrient depletion (Figure 2), suggesting that any dFe released from melting glacial ice near the sea surface may have been diluted by vertical mixing and/or assimilated by phytoplankton. Consistent with this interpretation, pFe concentrations over the upper 100 m near the Ross Ice Shelf averaged 4.1 ± 1.2 nM, which is slightly higher than the shelf-wide mean of 2.9 ± 2.6 nM, although significantly less than pFe concentrations reported for waters near glacial ice shelves in the Amundsen Sea [*Gerringa et al*., 2012; *Planquette et al*., 2013].

4.1.2. Iron in Circumpolar Deep Water and Modified Circumpolar Deep Water

Orsi and Wiederwohl [2009] define CDW and MCDW using a neutral density of $28.0 < \gamma^n < 28.27$ kg m^{-3}. Following *Dinniman et al*. [2011] we distinguish between the two by defining CDW as water sampled north of the shelf break, with temperature >0°C. Given the relatively high dFe concentrations previously reported for CDW [*Klunder et al*., 2011; *Sedwick et al*., 2011], relative to Ross Sea surface waters, and the potential for MCDW to entrain iron from sediments as it flows over the shelf, it has been suggested that vertical mixing of MCDW provides episodic inputs of dFe to the euphotic zone during the growing season [*Sedwick et al*., 2011]. Using an end-member of dFe concentration of 0.27 nM for MCDW based on samples collected during PRISM, *McGillicuddy et al*. [2015] estimated that MCDW accounts for around 17% of the annual dFe supply to the Ross Sea surface waters.

The CDW was detected at all three off-shelf stations, at depths of below 300 m at stations 1 and 2 and below 420 m at station 3 (Figures 2 and 3). Concentrations of dFe within this CDW endmember averaged 0.34 ± 0.08 nM ($n = 16$), which is slightly lower than the 0.47 nM measured further north of the shelf [*Sedwick et al*., 2011] and the average value of ~0.5 nM reported for the Atlantic sector of the Southern Ocean [*Klunder et al*., 2011], but is consistent with values of 0.33–0.34 nM dFe reported for CDW at an off-shelf station north of Joides Trough [*Hatta et al*., 2017]. Particulate iron concentrations in CDW were relatively low (1.6 ± 0.5 nM; Table 2), presumably due to its off-shelf provenance and consequent low recent inputs of sedimentary or sinking biological material. The resulting relatively high contribution to total iron from dFe (18.7 ± 4.0%, compared to the overall average of 6.6 ± 5.3%) suggests that intrusions of CDW supply dFe, but little pFe, onto the Ross Sea shelf.

Of our three off-shelf stations, station 3, nearest the shelf, had notably higher CDW dFe concentrations (0.45 ± 0.03 nM, $n = 5$) than stations 1 and 2 (0.29 ± 0.02 nM, $n = 11$; Figure 7b). Station 3 also had higher pFe concentrations in CDW, particularly in the large size fraction (1.5 ± 0.4 nM at station 3, compared to 0.7 ± 0.2 nM at stations 1 and 2), and the uppermost CDW and AASW at station 3 was also colder, fresher, and higher in dissolved oxygen than the stations further off-shelf. Together with the location of station 3 closer to the shelf break, this may indicate that, unlike at the two stations farther offshore, CDW sampled at station 3 had undergone significant interaction with shelf waters during circulation around the continental margin.

Some MCDW was detected at most of our on-shelf stations, usually over a narrow depth range. Its proximity to the surface ranged from 25 to 440 m depth (Figure 7b). The warmest and most oxygen deficient MCDW was observed above Mawson Bank along two transects across the Joides Trough (Figure 2), consistent with this water being derived from CDW that had recently intruded on to the shelf and mixed with shelf waters [*Dinniman et al*., 2011; *Kohut et al*., 2013]. Above Mawson Bank, at stations 85 and 86, a thick and apparently well-mixed layer of MCDW extended from ~150 m depth down to the crest of the bank (Figure 7b), and displayed some of the highest dFe concentrations measured in MCDW (0.24–0.26 nM), along with pFe concentrations of 1.5–2.7 nM. In contrast, over Pennell Bank, MCDW was restricted to a much thinner layer over the western flank, which was not sampled for dFe, and AASW extended down to the crest (stations 79 and 92; see first and last stations of section F in Figure 7a). Although the dFe concentrations above Pennell Bank at these two stations were similar to Mawson Bank (0.22–0.24 nM), pFe concentrations at station 79 were higher, increasing with depth from 2.7 nM at 130 m to 7.8 nM at 240 m. A similar contrast between water masses and iron distributions over these two banks in a previous study was attributed to the presence of MCDW over Mawson Bank increasing the near-bottom density gradient and reducing vertical mixing of sediments above the bank [*Hatta et al*., 2017].

In the southwestern corner of the Ross Sea, water identified as MCDW was colder (–1.9 to −1.6°C) and mostly confined to the upper 200 m. Here concentrations of dFe in MCDW were generally low relative to the CDW (0.14 ± 0.06 nM; $n = 69$), with the exception of six samples with MCDW characteristics collected

from shallow stations close to Franklin Island (mean = 0.42 ± 0.05 nM). Excluding these six samples, dFe concentrations in CDW and MCDW followed a trend of lower values in colder, fresher waters, presumably reflecting the mixing of CDW with dFe-poor AASW as it moves on to the continental shelf, as well as the biological removal of dFe where the MCDW shoals into the euphotic zone.

4.1.3. Iron in Shelf Water and Modified Shelf Water

At numerous stations in the southwestern Ross Sea, most of the water column below ~100 m was accounted for by SW, defined by $\gamma^n > 28.27$ kg m^{-3} and potential temperature (θ) of −1.95 to −1.85°C, and by MSW ($\gamma^n > 28.27$ kg m^{-3}, $\theta > -1.85$°C). In other areas, such as over the flanks of Ross Bank and at the easternmost stations, these water masses were represented in only the deepest 100–200 m of the water column (Figures 7c, 7e, and 7f). Concentrations of dFe and pFe in SW were, on average, higher than those in MCDW, but showed greater variability, with ranges of 0.06–2.19 nM dFe and 0.93–57.3 nM pFe, likely reflecting localized benthic inputs of both dFe and pFe. The MSW (Figure 7c) and LSSW (S < 34.62; Figure 7e) had dFe and pFe concentrations comparable to MCDW, whereas the HSSW (S > 34.62; Figure 7f), which accounted for near-bottom waters, including benthic nepheloid layers [*Marsay et al*., 2014], had significantly higher concentrations of both dFe and pFe (Table 2).

The dense HSSW, which is observed over much of the water column in the southwestern Ross Sea and in other deeper areas of the shelf, is exported offshore at the northwestern edge of the shelf [*Padman et al*., 2009], and thus likely contributes both dFe and pFe to the Antarctic Bottom Water. Doming of the pycnocline associated with the core of a cyclonic eddy surveyed in the southwestern Ross Sea brought HSSW to within 150 m of the surface, compared to ~300 m at a station on the edge of the eddy, and resulted in elevated dFe concentrations from 200 to 600 m depth (Figure 7f and supporting information Figure S2), demonstrating the potential of such mesoscale features to introduce iron into Ross Sea near-surface waters. The HSSW is also thought to represent a major source of iron to surface waters during deep convective mixing in the winter [*McGillicuddy et al*., 2015].

4.1.4. Iron in Ice Shelf Water

The ISW is formed when waters flow under the Ross Ice Shelf, are cooled and freshened via the melting of basal ice, and then flow northward in plumes with a characteristic potential temperature of $\theta < -1.95$°C [*Orsi and Wiederwohl*, 2009; *Smethie and Jacobs*, 2005]. As such, it has been suggested that the interaction with basal glacial ice may result in ISW being enriched in dFe and pFe, some of which may reach the euphotic zone in the polynya [*Fitzwater et al*., 2000; *Herraiz-Borreguero et al*., 2016; *Sedwick et al*., 2011]. However, recent model simulations of meltwater released from the Ross Ice Shelf suggest that glacial meltwater, including that carried in ISW, can account for only a small fraction of the dFe supplied to Ross Sea surface waters over an annual cycle [*McGillicuddy et al*., 2015].

Stations 56–71 were occupied close to the Ross Ice Shelf between 177.8°E and 178.8°W, with the aim of sampling ISW that is advected northward from the ice shelf, and the defining temperature minimum was detected at various depths ranging between 205 and 628 m (Figure 2). Minor amounts of ISW were also identified at stations over the southern and eastern slopes of Ross Bank, and within the southwestern Ross Sea (Figure 7d). Concentrations of dFe associated with the ISW were higher than in Ross Sea surface waters, at 0.13–0.36 nM (Figures 3 and 7d), and represented subsurface maxima at 330–400 m depth in the dFe profiles of stations 58 and 62 (Figure 4). However, the mean dFe concentration of ISW (0.24 ± 0.07 nM) was statistically indistinguishable from non-ISW samples (typically HSSW) in the same depth range at on-shelf stations (0.19 ± 0.10 nM, $n = 62$; Figure 7f). Concentrations of pFe in ISW were relatively low, averaging 2.7 ± 1.5 nM, resulting in a relatively high contribution of dFe to total iron in ISW (10.6 ± 3.5%; Table 2).

4.2. The Influence of Islands and Coastline

Away from the Antarctic continental shelf, some of the highest chlorophyll concentrations in the Southern Ocean are observed around island platforms such as Kerguelen, Crozet, and South Georgia, where seafloor sediments are much closer to the surface ocean. This "island mass effect" leads to elevated dFe concentrations in downstream surface waters, relative to the surrounding ocean [*Blain et al*., 2001; *Korb and Whitehouse*, 2004; *Pollard et al*., 2009]. We saw similarly elevated dFe concentrations in the Ross Sea at two stations close to Franklin Island (Figure 4, stations 101 and 101a), each located ~4 km southwest of the island and separated from each other by ~1 km. The two stations had very different dFe concentration profiles compared to other stations on the shelf, with elevated dFe concentrations throughout the upper 100 m (0.20–0.50 nM). Moreover, the two profiles were also different from each other; the more northerly

station 101 displayed an almost linear increase in dFe concentration with depth to the deepest sample collected (111 m, 13 m above the seafloor), whereas dFe concentrations at station 101a were more homogeneous, ranging from 0.42 to 0.48 nM, consistent with the less stratified water column evident from CTD data. Particulate iron concentrations were only measured at station 101a, with pFe below 20 m elevated relative to most other stations (Figure 5).

Both stations were in partially ice-covered waters at the time of sampling, and while release of iron from melting sea ice may have contributed to the overall enhanced dFe concentrations, the lack of a specific dFe maximum in the fresher surface waters, combined with the shallow bathymetry, suggests a sedimentary iron source in each case. *Gerringa et al*. [2015] also collected samples near Franklin Island, noting a decrease in subsurface dFe concentrations along a west to east transect from the island, from which they estimated a horizontal dFe flux from the island platform. While no such transect was performed during the PRISM study, we note that the dFe profile at our station 102, located close to transect station 90 of *Gerringa et al*. [2015], had a subsurface maximum of ~0.17 nM at 70–100 m depth (Figure 4). This feature, which is absent from profiles further from the island, may represent an advective transport of dFe derived from sediments surrounding Franklin Island to nearby waters.

A similar enrichment in dFe was seen below 100 m depth at station 116 (Figure 4), which was located in 575 m of water ~30 km east of the coast of Victoria Land, and to a lesser extent at stations 115 and 114, progressively further offshore from the coast. Here the subsurface dFe profiles appear to be influenced by a combination of local seafloor sediment sources (evidenced by the 2.19 nM dFe concentration 16 m above the bottom at station 116) and sedimentary dFe advected from the nearby coastline (supported by the elevated concentrations in the 100–400 m depth range). The shallow coastal waters of Victoria Land and Ross Island, along with Franklin and Beaufort Islands, may thus represent important local sources of iron to the western Ross Sea during the summer months, in a similar way that shallow banks have been suggested as dFe sources on the Ross Sea shelf [*Marsay et al*., 2014]. The shoaling pycnocline associated with the eddy at station 10, and the corresponding elevated dFe concentrations at depth (see section 4.1.3), imply that such mesoscale features can potentially deliver iron from these coastal sources to surface waters within the polynya during the summer months.

4.3. The Nature of Particulate Iron in the Ross Sea

Particles are a key component of the biogeochemical cycling of iron in the ocean [*Abadie et al*., 2017; *Boyd and Ellwood*, 2010; *Milne et al*., 2017], and in this study average concentrations of both small and large pFe were greater than dFe concentration at all depths (Figure 8b). Particulate iron introduced to surface waters of the Antarctic shelf seas may include lithogenic material in atmospheric dust, sediments transported from the coast by drifting sea ice, and glacial debris released from icebergs and ice shelves [*de Jong et al*., 2013; *Raiswell*, 2011; *Winton et al*., 2014]. Some fraction of this lithogenic pFe may undergo dissolution in the euphotic zone and become available for biological uptake, while some may be directly accessed from the particulate phase [*Boyd and Ellwood*, 2010; *Frew et al*., 2006], and biogenic pFe can also be recycled before sinking out of the upper ocean [*Strzepek et al*., 2005]. Iron can also be transformed from the dissolved to the particulate phase, via biological uptake, scavenging by particulate material, or formation of authigenic particles. Sinking particles carry pFe deeper into the water column, where remineralization and dissolution may release dFe, or additional dFe may be scavenged [*Abadie et al*., 2017; *Boyd et al*., 2010].

The relative importance of these processes influence both the depth profile of dFe and the ratio of dFe to macronutrients in subsurface waters [*Boyd and Ellwood*, 2010]. The distribution of different forms of pFe may therefore provide information concerning the importance of recycling versus the supply of new iron in supporting primary production. In this section, we characterize pFe in the Ross Sea by considering total pFe as the sum of biogenic (pFe_{bio}), lithogenic (pFe_{lith}), and authigenic and/or scavenged (pFe_{auth}) fractions, which are determined by considering the distribution of pFe in relation to particulate phosphorus and aluminum. We show that pFe_{bio} concentrations in surface waters contribute significantly to the pool of biologically available iron and that pFe_{auth} close to the seafloor may contribute to biologically available iron supplied to surface waters during wintertime convective mixing. We also compare the distributions of these pFe fractions to those for pMn, showing pMn_{auth} to be distributed higher in the water column than pFe_{auth}.

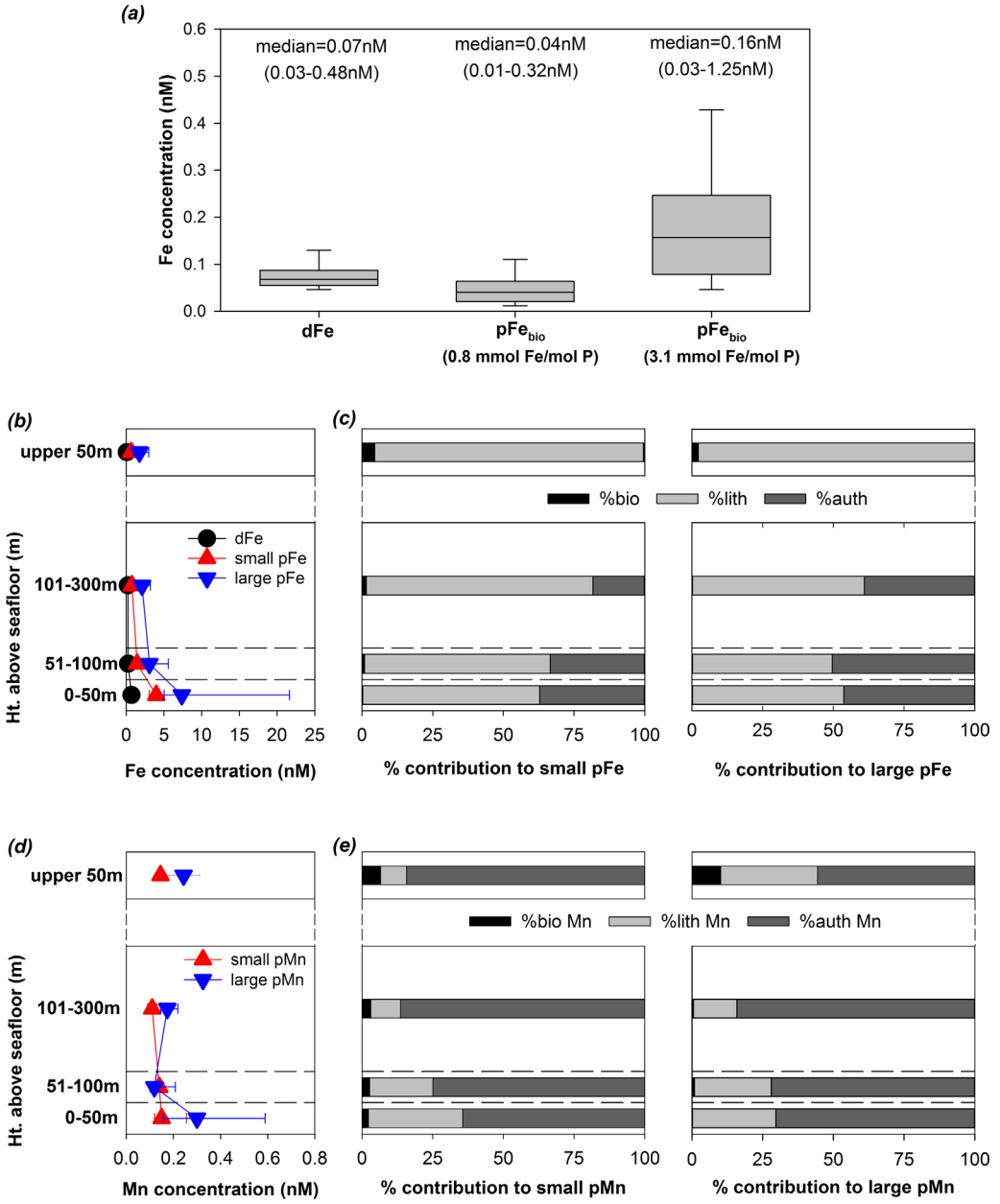

Figure 8. (a) Upper 50 m dFe concentrations compared to pFe_{bio} concentrations calculated using Fe/P ratios of 0.8 and 3.1 mmol mol^{-1}. Each box spans 25th to 75th percentiles and is bisected by median value. Whiskers span 10th to 90th percentiles. (b) Median (and 25th to 75th percentile) concentrations of dFe, small and large pFe in surface waters and in height intervals above the seafloor. (c) Median percentage contributions of pFe_{bio}, pFe_{lith}, and pFe_{auth} to small and large pFe in the same intervals. (d) As for Figure 8b, for small and large pMn. (e) As for Figure 8c, for small and large pMn.

4.3.1. Particulate Phosphorus and Biological Iron

The pFe/pP ratio in both size classes increases toward the seafloor (Figures 6a and 6b and supporting information Table S1). This is due to the main constraints on pP distribution being production of organic material in surface waters and remineralization below the euphotic zone, releasing dissolved phosphorus-containing compounds, whereas pFe distribution is also affected by lithogenic and authigenic contributions. In addition, dFe released during remineralization of biogenic material may subsequently be scavenged back to the particulate phase by sinking particles or resuspended sediments.

Twining and Baines [2013] report a cellular Fe/P ratio for Fe-limited Southern Ocean diatoms of 1.5 mmol mol^{-1}, with taxon-specific values of 0.8 mmol mol^{-1} for pennate diatoms and 3.1 mmol mol^{-1} for centric

diatoms. Assuming that all pP is associated with cellular material, we use this range of values along with pP data to calculate the contribution made by pFe_{bio} to total pFe. These calculations involve a number of caveats. First, we do not know the cellular Fe/P ratios for *Phaeocystis antarctica*, which is one of the most abundant phytoplankton in the Ross Sea. However, studies during PRISM suggest that despite its abundance, *P. antarctica* contributed a minor amount to carbon biomass relative to diatoms [*Mosby and Smith*, 2015]. Second, it is possible that pP, and therefore pFe_{bio}, is underestimated due to losses of labile material during filtering and rinsing [*Collier and Edmond*, 1984; *Twining et al*., 2015], although the use of small volumes of a rinse solution at a pH close to that of seawater was designed to minimize such loss. Third, the Fe/P ratios used represent intracellular values for living phytoplankton and may not account for all of the pFe associated with biogenic material in this study, as remineralization of this material results in cellular P being released into the dissolved phase while cellular iron may be rescavenged back onto particles. Thus, particularly in the upper 50 m, *biologically available* pFe may exceed the pFe_{bio} values we have calculated.

Using this cellular pFe/pP range of 0.8–3.1 mmol mol^{-1}, our calculated pFe_{bio} concentrations (both size classes combined) span <0.01–1.25 nM ($n = 202$), with highest values in surface waters. Median values calculated for the upper 50 m (0.04 nM using 0.8 mmol mol^{-1}; 0.16 nM using 3.1 mmol mol^{-1}; $n = 101$) are 60 and 233% of the median dFe concentration, respectively (0.07 nM; Figure 8a). This indicates that consideration of pFe_{bio} significantly increases the pool of biologically available Fe in Ross Sea surface waters, assuming it is not lost from the mixed layer before it can be recycled.

Indeed, the rapid recycling of pFe_{bio} in surface waters [*Boyd and Ellwood*, 2010; *Strzepek et al*., 2005] may help account for the continued high rates of primary production observed in the Ross Sea during summer, despite low dFe concentrations [*Sedwick et al*., 2011]. Although this scenario may seem at odds with the relatively high *f* ratio estimated for the Ross Sea [*Asper and Smith*, 1999], the biological cycling of Fe should be distinguished from the cycling of N, which is used to define the *f* ratio [*Boyd et al*., 2017]. Conceivably, the cycling of Fe in the Ross Sea may instead be characterized by low "*fe*" ratios, (uptake of new iron/uptake of new and regenerated iron), similar to values estimated for high nutrient low chlorophyll waters during the FeCycle study [*Boyd et al*., 2005]. In addition, the particulate material collected during PRISM likely undersampled the larger (>10 μm) sinking particles that represent the greatest fraction of pFe exported from Ross Sea surface waters [*Bochdansky et al*., 2017; *Frew et al*., 2006; *Smith et al*., 2017]; indirect evidence in support of this suggestion is described in section 4.3.2.

Using a 1.5 mmol mol^{-1} Fe/P ratio averaged for all Southern Ocean diatoms [*Twining and Baines*, 2013], we calculated pFe_{bio} to account for as much as 30% of total pFe in some surface water samples, thought it averaged 5.8 and 2.5% of small and large pFe inventories, respectively (Figure 8c). The calculated contribution from pFe_{bio} decreased with depth due to lower pP concentrations. From a bottom up perspective, the lowest contributions from pFe_{bio} were within 50 m of the seafloor (<0.6% of total pFe in all cases).

4.3.2. Contrasting Distributions of Lithogenic and Authigenic pFe and pMn

Median concentrations of pFe, pAl, and pMn were all highest near the seafloor in both size fractions (Figure 5 and supporting information Table S1), likely reflecting the significant influence of resuspended sediments for these elements. The similarity of measured pFe/pAl throughout the water column (Figures 6a and 6b) to average UCC and local sediment values suggests that much of the pFe in the water column was lithogenic material, consistent with the generally low contributions calculated for pFe_{bio}. Surprisingly, pFe/pAl was *lowest* in the upper 50 m and generally increased with proximity to the seafloor (Figures 6c and 6d and supporting information Table S1), reaching values that were enriched in iron relative to local surface sediments [*Angino*, 1966]. The lower pFe/pAl values in surface waters, including ~60 measurements in each size fraction that were lower than crustal values (i.e., <0.19 mol mol^{-1}) may indicate a biologically driven removal of some fraction of lithogenic pFe [*Barrett et al*., 2012; *Johnson et al*., 1997]. Alternatively, lower pFe/pAl ratios in the upper water column may result from uptake of dissolved Al and its incorporation within the structure of biogenic silica [*Gehlen et al*., 2002; *Van Bennekom et al*., 1991].

The apparent presence of Fe-depleted particles stands in contrast to previous results from the Ross Sea [*Coale et al*., 2005] and around the Kerguelen Islands [*van der Merwe et al*., 2015] where pFe/pAl ratios were significantly elevated relative to crustal values. However, our data are consistent with previous speculation that high Fe/Al measured in sinking biogenic particles collected in the Ross Sea may be balanced by Fe-depleted suspended lithogenic particles in the upper water column [*Collier et al*., 2000], as well as the transformation of pFe_{lith} to pFe_{bio} in the surface mixed layer before settling, as proposed by *Frew et al*. [2006].

This, however, raises the question of why both small and large fractions of particulate material were found to be depleted in Fe in our study.

We suggest that this apparent shortage of Fe-enriched particles may be an artefact of the relatively small volumes of water that were filtered for particulate material (averaging 3.4 L), compared to larger volumes (~50 to ~2000 L) filtered by others [*Coale et al*., 2005; *van der Merwe et al*., 2015]. Filtration of small volumes can lead to undersampling of large, sinking biogenic particles that might otherwise contribute to high pFe/pAl ratios. Additionally, the undersampling of large, fast-sinking particles when sampling from Niskin bottles and other samplers, in which the spigots are positioned 2–3 cm above the bottom of the sampler are well documented [e.g., *Gardner*, 1977].

Assuming a lithogenic Fe/Al ratio of 0.19 mol mol^{-1} [*Wedepohl*, 1995] and that all measured pAl was lithogenic, our pAl data were used to calculate the contribution of lithogenic iron (pFe_{lith}) to pFe. This yielded pFe_{lith} concentrations in the range of 0.62–35.6 nM, for the two size classes combined, with a median value of 2.2 nM ($n = 264$). Comparing pFe_{lith} to total pFe suggests that lithogenic Fe accounted for 30–271% of total pFe in the small size fraction (median 84%), and 30–1710% for the large size fraction (median 75%). Clearly, these estimates are very sensitive to the choice of the lithogenic Fe/Al ratio. Samples with Fe/Al $<$0.19 mol mol^{-1} yielded pFe_{lith} values $>$100%. Any contribution from nonlithogenic pAl, either through incorporation into biogenic silica or by scavenging of dissolved Al, would lead to overestimates of pFe_{lith}.

Despite this limitation, our approach yields useful information concerning the distribution of pFe_{lith}. In the upper 50 m, median concentrations of pFe_{lith} were calculated to be 0.6 and 3.1 nM in the small and large fractions, respectively. These values correspond to 95 and 132% of total pFe in each size fraction, although these are clearly overestimates, as pFe_{bio} must account for at least a small proportion of pFe in the euphotic zone (see section 4.3.1; Figure 8c). Although concentrations of pAl, and therefore pFe_{lith}, increased toward the seafloor, the Fe/Al also increased (supporting information Table S1 and Figure 6), resulting in the pFe_{lith} contribution to total pFe generally decreasing, to only 63 and 54% of the small and large size pFe, respectively, within 50 m of the seafloor (Figure 8c).

Thus, although lithogenic material contributes to the increased particle load in benthic nepheloid layers and can explain some of the increase in pFe concentration near the seafloor, it seems clear that authigenic and/or scavenged pFe becomes increasingly important closer to the seafloor. This is consistent with resuspension of authigenic Fe oxyhydroxides formed within the sediments and/or with scavenging onto the resuspended particles of elevated near-seafloor dFe concentrations, which in turn result from diffusion or other mobilization of the sediment pore waters into the water column [*Marsay et al*., 2014]. From the difference between measured pFe concentrations and estimates of pFe_{bio} and pFe_{lith}, we calculate that this pFe_{auth} contributes 0–70% of total pFe across all samples. In the upper 50 m of the water column, the median contribution of pFe_{auth} was calculated as zero, though this is likely to be an underestimate, given the depleted pFe/pAl ratios in near surface waters and resulting overestimation of pFe_{lith} (see above). The pFe_{auth} contribution was greatest close to the seafloor (median values of 37 and 46% for small and large pFe, respectively; Figure 8c). Recent studies have highlighted the importance of labile pFe phases in buffering dFe concentrations through reversible exchange [*John et al*., 2017; *Milne et al*., 2017]. Thus, any mobilization of this deep pFe_{auth} to the upper water column during deep, wintertime convective mixing could potentially provide an additional input of bioavailable iron at the start of the growing season.

Unlike pFe/pAl, measured pMn/pAl ratios were lowest within 50 m of the seafloor, where they were close to sedimentary values (supporting information Table S1). As with pFe, we estimated the lithogenic contribution to total pMn (pMn_{lith}) by multiplying pAl concentrations by the crustal Mn/Al molar ratio of 3.3×10^{-3} [*Wedepohl*, 1995]. Our calculations suggest that the pMn_{lith} contribution to pMn was much less than was the case for Fe, averaging only 12% (range 5–65%), and 18% (range 5–100%) in the small and large size fractions, respectively. The remaining pMn is presumed to be mostly authigenic, although a small contribution may come from pMn in biogenic material, which was calculated using a cellular Mn/P ratio for Southern Ocean diatoms of 5×10^{-4} mol mol^{-1} [*Twining and Baines*, 2013] and our pP data.

Unlike pFe_{lith}, the proportion of pMn_{lith} was greatest within 50 m of the seafloor (Figure 8e) and decreased with distance above the seafloor. As with pFe_{lith}, our pMn_{lith} estimates are very sensitive to the choice of Mn/Al for lithogenic material. And similarly, any scavenging of dissolved Al by particles or biogenic contribution to pAl is likely to result in an overestimate of the lithogenic fraction of pMn. Nevertheless, these

estimates reveal an apparent trend toward an increase in the relative proportion of authigenic pMn (pMn_{auth}), in both size fractions, with increased height above the seafloor.

The increase in contribution from pMn_{auth} (and pMn/pAl) with height above the seafloor (Figure 8e) may reflect a greater fraction of pMn higher in the water column being formed via bacterially mediated oxidation of dissolved Mn(II) to MnO_2 [*Tebo et al*., 2004]. As would be expected for this scenario, the impact is most pronounced in the small size fraction (supporting information Table S1). Nearer the seafloor, the greater concentration of resuspended sedimentary material in nepheloid layers increases both pMn and pAl concentrations and drives pMn/pAl ratios closer to sedimentary values. A similar pattern of higher pMn/pAl ratios with height above the seafloor was reported by *Planquette et al*. [2013] for the Amundsen Sea.

Davidson and Marchant [1987] have demonstrated that the mucus surrounding *Phaeocystis* colonies can also promote oxidation and precipitation of Mn(II), which would also be expected to increase pMn/pAl ratios in the large size fraction in surface waters. Evidence of this process is not seen in our data (supporting information Table S1), which may reflect the relatively low pMn concentrations measured, or again represent an artefact due to the undersampling of large ($>$10 μm) biogenic particles, which would include *P. antarctica* colonies. However, we note that the Mn/Al ratios of particulate material collected by in situ pumps near Kerguelen Island by *van der Merwe et al*. [2015] also showed no Mn enrichment.

Our calculations suggest that distributions of both pFe and pMn in the Ross Sea water column appear to be influenced by an authigenic and/or scavenged component. This contribution seems to be more important for the inventory of pMn than for pFe, as revealed by the calculated average contributions of authigenic pMn and pFe to totals (85 versus 17%, respectively; Figure 8). Furthermore, the distributions of pMn_{auth} and pFe_{auth} are different. The relative proportion of pFe_{auth} is greatest near the seafloor, and likely dominated by resuspension of authigenic pFe in the sediments and by scavenging of dFe released from sediment pore water into the water column during resuspension of material. In contrast, the relative proportion of pMn_{auth} is greatest higher in the water column, away from the influence of resuspended sedimentary pMn. These differences are evident in the pMn/pFe distribution, which increases with height above the seafloor from values close to local surface sediments (0.039 mol mol^{-1} [*Angino*, 1966]) to average values $>$0.1 mol mol^{-1} in both size fractions in the upper 50 m (supporting information Table S1).

5. Conclusions

The distribution of dFe over the Ross Sea shelf during the PRISM project is consistent with the results of previous studies, showing widespread low concentrations ($\sim$0.1 nM) of this essential micronutrient in surface waters during midsummer. Only a small number of stations in or near shallower water, or near areas of melting sea ice showed surface dFe concentrations $>$0.1 nM. However, not all areas of recent sea ice melt showed elevated dFe concentrations, suggesting rapid uptake of ice-derived dFe during bloom conditions and/or release of dFe prior to complete melting of the seasonal pack ice. An apparent decrease in the dFe concentration in MCDW as it moves further onto the shelf and shoals suggests that mixing with overlying waters may constitute a modest supply of dFe to the euphotic zone, as has been suggested by previous field observations [*Sedwick et al*., 2011] and numerical modelling [*Dinniman et al*., 2011].

The PRISM cruise was able to collect samples for dFe and pFe analysis that are representative of all major water mass types in the Ross Sea [*Orsi and Wiederwohl*, 2009], identifying potential end-member dFe concentrations for two proposed sources in CDW and ISW. We show that during mid-summer a large proportion of the water column dFe inventory is associated with deep, dense shelf waters, which highlights the importance of winter convective overturn in supplying dFe to the euphotic zone for the following growing season [see, e.g., *McGillicuddy et al*., 2015]. Our results also point to the potential importance of mesoscale features in transporting dFe in deeper waters to the euphotic zone during the summer months.

Our results highlight the potential significance of recycled iron in fueling phytoplankton production in the Ross Sea polynya over the mid to late summer. Measured pFe concentrations were always greater than those of dFe, and we suggest that biogenic pFe represents a pool of biologically available iron that is comparable in concentration to dFe in Ross Sea surface waters, despite our likely undersampling of larger, Fe-rich particles.

Elevated concentrations of dFe and particulate Fe, Al, and Mn in association with benthic nepheloid layers highlight the likely influence of sediment resuspension and release of sedimentary pore fluids on the vertical distributions of these elements. Lithogenic material appears to account for most of the pFe throughout the water column, with an increasing contribution from authigenic or scavenged iron toward the seafloor. In contrast, the relative authigenic contribution to pMn becomes more important as concentrations decrease with height above the seafloor, highlighting differences in biogeochemistry between the two elements.

Acknowledgments

All data used herein are available at the Biological and Chemical Oceanography Data Management Office: http://www.bco-dmo.org/project/2155. Support of this research by the National Science Foundation's United States Antarctic Program is gratefully acknowledged (awards ANT-0944174 to P.N.S. and ANT-0944165 to D.J.M.). P.M.B. was also funded by National Science Foundation award OCE-0649505 to J. Resing. This is JISAO publication #2017–073 and PMEL publication #4652. The authors gratefully acknowledge Bettina Sohst, Candace Wall, and Jennifer Bennett for assistance with collection, processing, and analysis of water samples, and Walker Smith Jr., for chlorophyll measurements and constructive comments. We also thank the other members of the PRISM science team, the officers and crew of the RVIB *Nathaniel B. Palmer*, and the support personnel of Raytheon Polar Services Company for their contributions to this work. Ocean Data View [*Schlitzer*, 2017] was used to produce several of the figures and for data analysis in this manuscript.

References

Abadie, C., F. Lacan, A. Radic, C. Pradoux, and F. Poitrasson (2017), Iron isotopes reveal distinct dissolved iron sources and pathways in the intermediate versus deep Southern Ocean, *Proc. Natl. Acad. Sci. U. S.* A., *114*(5), 858–863, doi:10.1073/pnas.1603107114.

Angino, E. E. (1966), Geochemistry of Antarctic pelagic sediments, *Geochim. Cosmochim. Acta*, *30*(9), 939–961, doi:10.1016/0016-7037(66)90029-9.

Arrigo, K. R., D. L. Worthen, and D. H. Robinson (2003), A coupled ocean-ecosystem model of the Ross Sea: 2. Iron regulation of phytoplankton taxonomic variability and primary production, *J. Geophys. Res.*, *108*(C7), 3231, doi:10.1029/2001JC000856.

Arrigo, K. R., G. van Dijken, and M. Long (2008a), Coastal Southern Ocean: A strong anthropogenic CO_2 sink, *Geophys. Res. Lett.*, *35*, L21602, doi:10.1029/2008GL035624.

Arrigo, K. R., G. L. van Dijken, and S. Bushinsky (2008b), Primary production in the Southern Ocean, 1997–2006, *J. Geophys. Res.*, *113*, C08004, doi:10.1029/2007JC004551.

Arrigo, K. R., G. L. van Dijken, and A. L. Strong (2015), Environmental controls of marine productivity hot spots around Antarctica, *J. Geophys. Res.*, *120*, 5545–5565, doi:10.1002/2015JC010888.

Asper, V. L., and W. O. Smith (1999), Particle fluxes during austral spring and summer in the southern Ross Sea, Antarctica, *J. Geophys. Res.*, *104*(C3), 5345–5359, doi:10.1029/1998JC900067.

Barrett, P. M., J. A. Resing, N. J. Buck, C. S. Buck, W. M. Landing, and C. I. Measures (2012), The trace element composition of suspended particulate matter in the upper 1000 m of the eastern North Atlantic Ocean: A16N, *Mar. Chem.*, *142*, 41–53, doi:10.1016/j.marchem.2012.07.006.

Blain, S., et al. (2001), A biogeochemical study of the island mass effect in the context of the iron hypothesis: Kerguelen Islands, Southern Ocean, *Deep Sea Res., Part I*, *48*(1), 163–187, doi:10.1016/S0967-0637(00)00047-9.

Bochdansky, A. B., M. A. Clouse, and D. A. Hansell (2017), Mesoscale and high-frequency variability of macroscopic particles (>100 μm) in the Ross Sea and its relevance for late-season particulate carbon export, *J. Mar. Syst.*, *166*, 120–131, doi:10.1016/j.jmarsys.2016.08.010.

Boyd, P. W., and M. J. Ellwood (2010), The biogeochemical cycle of iron in the ocean, *Nat. Geosci.*, *3*(10), 675–682, doi:10.1038/Ngeo964.

Boyd, P. W., et al. (2005), FeCycle: Attempting an iron biogeochemical budget from a mesoscale SF_6 tracer experiment in unperturbed low iron waters, *Global Biogeochem. Cycles*, *19*, GB4S20, doi:10.1029/2005GB002494.

Boyd, P. W., E. Ibisanmi, S. G. Sander, K. A. Hunter, and G. A. Jackson (2010), Remineralization of upper ocean particles: Implications for iron biogeochemistry, *Limnol. Oceanogr.*, *55*(3), 1271–1288, doi:10.4319/lo.2010.55.3.1271.

Boyd, P. W., M. J. Ellwood, A. Tagliabue, and B. S. Twining (2017), Biotic and abiotic retention, recycling and remineralization of metals in the ocean, *Nat. Geosci.*, *10*(3), 167–173, doi:10.1038/NGEO2876.

Brown, M. T., S. M. Lippiatt, M. C. Lohan, and K. W. Bruland (2012), Trace metal distributions within a Sitka eddy in the northern Gulf of Alaska, *Limnol. Oceanogr.*, *57*(2), 503–518, doi:10.4319/lo.2012.57.2.0503.

Bruland, K. W., E. L. Rue, G. J. Smith, and G. R. DiTullio (2005), Iron, macronutrients and diatom blooms in the Peru upwelling regime: Brown and blue waters of Peru, *Mar. Chem.*, *93*(2–4), 81–103, doi:10.1016/j.marchem.2004.06.011.

Cassar, N., M. L. Bender, B. A. Barnett, S. Fan, W. J. Moxim, H. Levy, and B. Tilbrook (2007), The Southern Ocean biological response to aeolian iron deposition, *Science*, *317*(5841), 1067–1070, doi:10.1126/science.1144602.

Coale, K. H., X. Wang, S. J. Tanner, and K. S. Johnson (2003), Phytoplankton growth and biological response to iron and zinc addition in the Ross Sea and Antarctic Circumpolar Current along 170°W, *Deep Sea Res., Part II*, *50*(3–4), 635–653, doi:10.1016/S0967-0645(02)00588-X.

Coale, K. H., R. M. Gordon, and X. Wang (2005), The distribution and behavior of dissolved and particulate iron and zinc in the Ross Sea and Antarctic circumpolar current along 170°W, *Deep Sea Res., Part I*, *52*(2), 295–318, doi:10.1016/j.dsr.2004.09.008.

Collier, R., and J. Edmond (1984), The trace element geochemistry of marine biogenic particulate matter, *Prog. Oceanogr.*, *13*(2), 113–199, doi:10.1016/0079-6611(84)90008-9.

Collier, R., J. Dymond, S. Honjo, S. Manganini, R. Francois, and R. Dunbar (2000), The vertical flux of biogenic and lithogenic material in the Ross Sea: Moored sediment trap observations 1996–1998, *Deep Sea Res., Part II*, *47*(15–16), 3491–3520, doi:10.1016/S0967-0645(00)00076-X.

Davidson, A. T., and H. J. Marchant (1987), Binding of manganese by Antarctic *Phaeocystis pouchetii* and the role of bacteria in its release, *Mar. Biol.*, *95*(3), 481–487, doi:10.1007/BF00409577.

Death, R., J. L. Wadham, F. Monteiro, A. M. Le Brocq, M. Tranter, A. Ridgwell, S. Dutkiewicz, and R. Raiswell (2014), Antarctic ice sheet fertilises the Southern Ocean, *Biogeosciences*, *11*(10), 2635–2643, doi:10.5194/bg-11-2635-2014.

de Jong, J., V. Schoemann, N. Maricq, N. Mattielli, P. Langhorne, T. Haskell, and J. L. Tison (2013), Iron in land-fast sea ice of McMurdo Sound derived from sediment resuspension and wind-blown dust attributes to primary productivity in the Ross Sea, Antarctica, *Mar. Chem.*, *157*, 24–40, doi:10.1016/j.marchem.2013.07.001.

Dinniman, M. S., J. M. Klinck, and W. O. Smith Jr. (2011), A model study of Circumpolar Deep Water on the West Antarctic Peninsula and Ross Sea continental shelves, *Deep Sea Res., Part II*, *58*(13–16), 1508–1523, doi:10.1016/j.dsr2.2010.11.013.

Edwards, R., and P. Sedwick (2001), Iron in East Antarctic snow: Implications for atmospheric iron deposition and algal production in Antarctic waters, *Geophys. Res. Lett.*, *28*(20), 3907–3910, doi:10.1029/2001GL012867.

Fitzwater, S. E., K. S. Johnson, R. M. Gordon, K. H. Coale, and W. O. Smith (2000), Trace metal concentrations in the Ross Sea and their relationship with nutrients and phytoplankton growth, *Deep Sea Res. Part II*, *47*(15–16), 3159–3179, doi:10.1016/s0967-0645(00)00063-1.

Frew, R. D., D. A. Hutchins, S. Nodder, S. Sañudo-Wilhelmy, A. Tovar-Sanchez, K. Leblanc, C. E. Hare, and P. W. Boyd (2006), Particulate iron dynamics during FeCycle in subantarctic waters southeast of New Zealand, *Global Biogeochem. Cycles*, *20*, GB1S93, doi:10.1029/2005GB002558.

Gardner, W. D. (1977), Incomplete extraction of rapidly settling particles from water samplers, *Limnol. Oceanogr.*, *22*(4), 764–768, doi:10.4319/lo.1977.22.4.0764.
Gehlen, M., L. Beck, G. Calas, A. M. Flank, A. J. Van Bennekom, and J. E. E. Van Beusekom (2002), Unraveling the atomic structure of biogenic silica: Evidence of the structural association of Al and Si in diatom frustules, *Geochim. Cosmochim. Acta*, *66*(9), 1601–1609, doi:10.1016/S0016-7037(01)00877-8.
Gerringa, L. J. A., A. C. Alderkamp, P. Laan, C. E. Thuróczy, H. J. W. De Baar, M. M. Mills, G. L. van Dijken, H. van Haren, and K. R. Arrigo (2012), Iron from melting glaciers fuels the phytoplankton blooms in Amundsen Sea (Southern Ocean): Iron biogeochemistry, *Deep Sea Res., Part II*, *71–76*, 16–31, doi:10.1016/j.dsr2.2012.03.007.
Gerringa, L. J. A., P. Laan, G. L. van Dijken, H. van Haren, H. J. W. De Baar, K. R. Arrigo, and A. C. Alderkamp (2015), Sources of iron in the Ross Sea Polynya in early summer, *Mar. Chem.*, *177*, 447–459, doi:10.1016/j.marchem.2015.06.002.
Hatta, M., C. I. Measures, K. E. Selph, M. Zhou, and W. T. Hiscock (2013), Iron fluxes from the shelf regions near the South Shetland Islands in the Drake Passage during the austral-winter 2006, *Deep Sea Res., Part II*, *90*, 89–101, doi:10.1016/j.dsr2.2012.11.003.
Hatta, M., C. I. Measures, P. J. Lam, D. C. Ohnemus, M. E. Auro, M. M. Grand, and K. E. Selph (2017), The relative roles of modified circumpolar deep water and benthic sources in supplying iron to the recurrent phytoplankton blooms above Pennell and Mawson Banks, Ross Sea, Antarctica, *J. Mar. Syst.*, *166*, 61–72, doi:10.1016/j.jmarsys.2016.07.009.
Herraiz-Borreguero, L., D. Lannuzel, P. van der Merwe, A. Treverrow, and J. B. Pedro (2016), Large flux of iron from the Amery Ice Shelf marine ice to Prydz Bay, East Antarctica, *J. Geophys. Res. Oceans*, *121*, 6009–6020, doi:10.1002/2016JC011687.
John, S. G., J. Helgoe, E. Townsend, T. Weber, T. DeVries, A. Tagliabue, K. Moore, P. J. Lam, C. M. Marsay, and C. Till (2017), Biogeochemical cycling of Fe and Fe stable isotopes in the Eastern Tropical South Pacific, *Mar. Chem.*, doi:10.1016/j.marchem.2017.06.003, in press.
Johnson, K. S., R. M. Gordon, and K. H. Coale (1997), What controls dissolved iron concentrations in the world ocean?, *Mar. Chem.*, *57*(3–4), 137–161, doi:10.1016/S0304-4203(97)00043-1.
Johnson, K. S., et al. (2007), Developing standards for dissolved iron in seawater, *Eos Trans. AGU*, *88*(11), 131–132, doi:10.1029/2007EO110003.
Klunder, M. B., P. Laan, R. Middag, H. J. W. De Baar, and J. C. van Ooijen (2011), Dissolved iron in the Southern Ocean (Atlantic sector), *Deep Sea Res., Part II*, *58*(25–26), 2678–2694, doi:10.1016/j.dsr2.2010.10.042.
Knap, A., A. Michaels, A. Close, H. Ducklow, and A. Dickson (Eds.) (1996), Protocols for the Joint Global Ocean Flux Study (JGOFS) core measurements, *JGOFS Rep. 19*, vi+170 pp., Reprint of the IOC Manuals and Guides No. 29, UNESCO, 1994, Paris.
Kohut, J. T., E. Hunter, and B. Huber (2013), Small-scale variability of the cross-shelf flow over the outer shelf of the Ross Sea, *J. Geophys. Res. Oceans*, *118*, 1863–1876, doi:10.1002/jgrc.20090.
Kohut, J. T., et al. (2017), Mesoscale variability of the summer bloom over the northern Ross Sea shelf: A tale of two banks, *J. Mar. Syst.*, *166*, 50–60, doi:10.1016/j.jmarsys.2016.06.009.
Korb, R. E., and M. Whitehouse (2004), Contrasting primary production regimes around South Georgia, Southern Ocean: Large blooms versus high nutrient, low chlorophyll waters, *Deep Sea Res., Part I*, *51*(5), 721–738, doi:10.1016/j.dsr.2004.02.006.
Kustka, A. B., et al. (2015), The roles of MCDW and deep water iron supply in sustaining a recurrent phytoplankton bloom on central Pennell Bank (Ross Sea), *Deep Sea Res., Part I*, *105*, 171–185, doi:10.1016/j.dsr.2015.08.012.
Lannuzel, D., V. Schoemann, J. de Jong, J. L. Tison, and L. Chou (2007), Distribution and biogeochemical behaviour of iron in the East Antarctic sea ice, *Mar. Chem.*, *106*(1–2), 18–32, doi:10.1016/j.marchem.2006.06.010.
Lannuzel, D., V. Schoemann, J. de Jong, L. Chou, B. Delille, S. Becquevort, and J. L. Tison (2008), Iron study during a time series in the western Weddell pack ice, *Mar. Chem.*, *108*(1–2), 85–95, doi:10.1016/j.marchem.2007.10.006.
Lannuzel, D., V. Schoemann, J. de Jong, B. Pasquer, P. van der Merwe, F. Masson, J. L. Tison, and A. Bowie (2010), Distribution of dissolved iron in Antarctic sea ice: Spatial, seasonal, and inter-annual variability, *J. Geophys. Res.*, *115*, G03022, doi:10.1029/2009JG001031.
Li, Y., D. J. McGillicuddy, M. S. Dinniman, and J. M. Klinck (2017), Processes influencing formation of low-salinity high-biomass lenses near the edge of the Ross Ice Shelf, *J. Mar. Sys.*, *166*, 108–119, doi:10.1016/j.jmarsys.2016.07.002.
Lin, H., S. Rauschenberg, C. R. Hexel, T. J. Shaw, and B. S. Twining (2011), Free-drifting icebergs as sources of iron to the Weddell Sea, *Deep Sea Res., Part II*, *58*(11–12), 1392–1406, doi:10.1016/j.dsr2.2010.11.020.
Marsay, C. M., P. N. Sedwick, M. S. Dinniman, P. M. Barrett, S. L. Mack, and D. J. McGillicuddy (2014), Estimating the benthic efflux of dissolved iron on the Ross Sea continental shelf, *Geophys. Res. Lett.*, *41*, 7576–7583, doi:10.1002/2014GL061684.
Martin, J. H., S. E. Fitzwater, and R. M. Gordon (1990), Iron deficiency limits phytoplankton growth in Antarctic waters, *Global Biogeochem. Cycles*, *4*(1), 5–12, doi:10.1029/GB004i001p00005.
Martin, J. H., R. M. Gordon, and S. E. Fitzwater (1991), The case for iron, *Limnol. Oceanogr.*, *36*(8), 1793–1802, doi:10.4319/lo.1991.36.8.1793.
McGillicuddy, D. J., et al. (2015), Iron supply and demand in an Antarctic shelf ecosystem, *Geophys. Res. Lett.*, *42*, 8088–8097, doi:10.1002/2015GL065727.
Measures, C. I., J. Yuan, and J. A. Resing (1995), Determination of iron in seawater by flow injection analysis using in-line preconcentration and spectrophotometric detection, *Mar. Chem.*, *50*(1–4), 3–12, doi:10.1016/0304-4203(95)00022-J.
Measures, C. I., M. T. Brown, K. E. Selph, A. Apprill, M. Zhou, M. Hatta, and W. T. Hiscock (2013), The influence of shelf processes in delivering dissolved iron to the HNLC waters of the Drake Passage, Antarctica, *Deep Sea Res., Part II*, *90*, 77–88, doi:10.1016/j.dsr2.2012.11.004.
Milne, A., C. Schlosser, B. D. Wake, E. P. Achterberg, R. Chance, A. R. Baker, A. Forryan, and M. C. Lohan (2017), Particulate phases are key in controlling dissolved iron concentrations in the (sub)tropical North Atlantic, *Geophys. Res. Lett.*, *44*, 2377–2387, doi:10.1002/2016gl072314.
Mosby, A. F., and W. O. Smith Jr. (2015), Phytoplankton growth rates in the Ross Sea, Antarctica, *Aquat. Microb. Ecol.*, *74*(2), 157–171, doi:10.3354/ame01733.
Orsi, A. H., and C. L. Wiederwohl (2009), A recount of Ross Sea waters, *Deep Sea Res., Part II*, *56*(13–14), 778–795, doi:10.1016/j.dsr2.2008.10.033.
Padman, L., S. L. Howard, A. H. Orsi, and R. D. Muench (2009), Tides of the northwestern Ross Sea and their impact on dense outflows of Antarctic Bottom Water, *Deep Sea Res., Part II*, *56*(13), 818–834, doi:10.1016/j.dsr2.2008.10.026.
Planquette, H., R. M. Sherrell, S. Stammerjohn, and M. P. Field (2013), Particulate iron delivery to the water column of the Amundsen Sea, Antarctica, *Mar. Chem.*, *153*, 15–30, doi:10.1016/j.marchem.2013.04.006.
Pollard, R. T., et al. (2009), Southern Ocean deep-water carbon export enhanced by natural iron fertilization, *Nature*, *457*(7229), 577–580, doi:10.1038/nature07716.
Prézelin, B. B., E. E. Hofmann, C. Mengelt, and J. M. Klinck (2000), The linkage between Upper Circumpolar Deep Water (UCDW) and phytoplankton assemblages on the west Antarctic Peninsula continental shelf, *J. Mar. Res.*, *58*(2), 165–202, doi:10.1357/002224000321511133.
Raiswell, R. (2011), Iceberg-hosted nanoparticulate Fe in the Southern Ocean: Mineralogy, origin, dissolution kinetics and source of bioavailable Fe, *Deep Sea Res., Part II*, *58*(11–12), 1364–1375, doi:10.1016/j.dsr2.2010.11.011.

Raiswell, R., M. Tranter, L. G. Benning, M. Siegert, R. De'ath, P. Huybrechts, and T. Payne (2006), Contributions from glacially derived sediment to the global iron (oxyhydr)oxide cycle: Implications for iron delivery to the oceans, *Geochim. Cosmochim. Acta*, *70*(11), 2765–2780, doi:10.1016/j.gca.2005.12.027.

Ryan-Keogh, T. J., L. M. DeLizo, W. O. Smith Jr., P. N. Sedwick, D. J. McGillicuddy Jr., C. M. Moore, and T. S. Bibby (2017), Temporal progression of photosynthetic-strategy in phytoplankton in the Ross Sea, Antarctica, *J.* Mar. *Syst.*, *166*, 87–96, doi:10.1016/j.jmarsys.2016.08.014.

Schallenberg, C., P. van der Merwe, F. Chever, J. T. Cullen, D. Lannuzel, and A. R. Bowie (2016), Dissolved iron and iron(II) distributions beneath the pack ice in the East Antarctic (120°E) during the winter/spring transition, *Deep Sea Res., Part II*, *131*, 96–110, doi:10.1016/j.dsr2.2015.02.019.

Schlitzer, R. (2017), Ocean data view. [Available at http://odv.awi.de]

Sedwick, P. N., and G. R. DiTullio (1997), Regulation of algal blooms in Antarctic shelf waters by the release of iron from melting sea ice, *Geophys. Res. Lett.*, *24*(20), 2515–2518, doi:10.1029/97GL02596.

Sedwick, P. N., G. R. DiTullio, and D. J. Mackey (2000), Iron and manganese in the Ross Sea, Antarctica: Seasonal iron limitation in Antarctic shelf waters, *J. Geophys. Res.*, *105*(C5), 11,321–11,336, doi:10.1029/2000JC000256.

Sedwick, P. N., T. M. Church, A. R. Bowie, C. M. Marsay, S. J. Ussher, K. M. Achilles, P. J. Lethaby, R. J. Johnson, M. M. Sarin, and D. J. McGillicuddy (2005), Iron in the Sargasso Sea (Bermuda Atlantic Time-series Study region) during summer: Eolian imprint, spatiotemporal variability, and ecological implications, *Global Biogeochem. Cycles*, *19*, GB4006, doi:10.1029/2004GB002445.

Sedwick, P. N., et al. (2011), Early season depletion of dissolved iron in the Ross Sea polynya: Implications for iron dynamics on the Antarctic continental shelf, *J. Geophys. Res.*, *116*, C12019, doi:10.1029/2010JC006553.

Shadwick, E. H., B. Tilbrook, and G. D. Williams (2014), Carbonate chemistry in the Mertz Polynya (East Antarctica): Biological and physical modification of dense water outflows and the export of anthropogenic CO_2, *J. Geophys. Res.*, *119*, 1–14, doi:10.1002/2013JC009286.

Sherrell, R. M., M. E. Lagerström, K. O. Forsch, S. E. Stammerjohn, and P. L. Yager (2015), Dynamics of dissolved iron and other bioactive trace metals (Mn, Ni, Cu, Zn) in the Amundsen Sea Polynya, Antarctica, *Elem. Sci. Anth.*, *3*(1), 000071, doi:10.12952/journal.elementa.000071.

Smethie, W. M., and S. S. Jacobs (2005), Circulation and melting under the Ross Ice Shelf: Estimates from evolving CFC, salinity and temperature fields in the Ross Sea, *Deep Sea Res., Part I*, *52*(6), 959–978, doi:10.1016/j.dsr.2004.11.016.

Smith, W. O., J. Marra, M. R. Hiscock, and R. T. Barber (2000), The seasonal cycle of phytoplankton biomass and primary productivity in the Ross Sea, Antarctica, *Deep Sea Res., Part II*, *47*(15), 3119–3140, doi:10.1016/S0967-0645(00)00061-8.

Smith, W. O., P. N. Sedwick, K. R. Arrigo, D. G. Ainley, and A. H. Orsi (2012), The Ross Sea in a sea of change, *Oceanography*, *25*(3), 90–103, doi:10.5670/oceanog.2012.80.

Smith, W. O., D. J. McGillicuddy, E. B. Olson, V. Kosnyrev, E. E. Peacock, and H. M. Sosik (2017), Mesoscale variability in intact and ghost colonies of *Phaeocystis antarctica* in the Ross Sea: Distribution and abundance, *J. Mar. Syst.*, *166*, 97–107, doi:10.1016/j.jmarsys.2016.05.007.

Strzepek, R. F., M. T. Maldonado, J. L. Higgins, J. Hall, K. Safi, S. W. Wilhelm, and P. W. Boyd (2005), Spinning the "Ferrous Wheel": The importance of the microbial community in an iron budget during the FeCycle experiment, *Global Biogeochem. Cycles*, *19*, GB4S26, doi:10.1029/2005GB002490.

Tagliabue, A., and K. R. Arrigo (2005), Iron in the Ross Sea: 1. Impact on CO_2 fluxes via variation in phytoplankton functional group and non-Redfield stoichiometry, *J. Geophys. Res.*, *110*, C03009, doi:10.1029/2004JC002531.

Takahashi, T., et al. (2009), Climatological mean and decadal change in surface ocean pCO_2, and net sea-air CO_2 flux over the global oceans, *Deep Sea Res., Part II*, *56*(8–10), 554–577, doi:10.1016/j.dsr2.2008.12.009.

Tebo, B. M., J. R. Bargar, B. G. Clement, G. J. Dick, K. J. Murray, D. Parker, R. Verity, and S. M. Webb (2004), Biogenic manganese oxides: Properties and mechanisms of formation, *Annu. Rev. Earth Planet. Sci.*, *32*, 287–328, doi:10.1146/annurev.earth.32.101802.120213.

Twining, B. S., and S. B. Baines (2013), The trace metal composition of marine phytoplankton, *Annu. Rev. Mar. Sci.*, *5*, 191–215, doi:10.1146/annurev-marine-121211-172322.

Twining, B. S., S. Rauschenberg, P. L. Morton, D. C. Ohnemus, and P. J. Lam (2015), Comparison of particulate trace element concentrations in the North Atlantic Ocean as determined with discrete bottle sampling and in situ pumping, *Deep Sea Res., Part II*, *116*, 273–282, doi:10.1016/j.dsr2.2014.11.005.

Van Bennekom, A. J., A. G. J. Buma, and R. F. Nolting (1991), Dissolved aluminium in the Weddell-Scotia Confluence and effect of Al on the dissolution kinetics of biogenic silica, *Mar. Chem.*, *35*(1–4), 423–434, doi:10.1016/S0304-4203(09)90034-2.

van der Merwe, P., et al. (2015), Sourcing the iron in the naturally fertilised bloom around the Kerguelen Plateau: Particulate trace metal dynamics, *Biogeosciences*, *12*(3), 739–755, doi:10.5194/bg-12-739-2015.

Wadley, M. R., T. D. Jickells, and K. J. Heywood (2014), The role of iron sources and transport for Southern Ocean productivity, *Deep Sea Res., Part I*, *87*, 82–94, doi:10.1016/j.dsr.2014.02.003.

Wedepohl, K. H. (1995), The composition of the continental crust, *Geochim. Cosmochim. Acta*, *59*(7), 1217–1232, doi:10.1016/0016-7037(95)00038-2.

Winton, V. H. L., G. B. Dunbar, N. A. N. Bertler, M. A. Millet, B. Delmonte, C. B. Atkins, J. M. Chewings, and P. Andersson (2014), The contribution of aeolian sand and dust to iron fertilization of phytoplankton blooms in southwestern Ross Sea, Antarctica, *Global Biogeochem. Cycles*, *28*, 423–436, doi:10.1002/2013GB004574.